ACS APPLIED MATERIALS & INTERFACES

www.acsami.org

Research Article

Vascular Endothelial Growth Factor Receptor 1 Targeting Fusion Polypeptides with Stimuli-Responsiveness for Anti-angiogenesis

Min Jeong Kang, Kug-Hwan Roh, Jae Sang Lee, Jae Hee Lee, SaeGwang Park,* and Dong Woo Lim*

Cite This: *ACS Appl. Mater. Interfaces* 2023, 15, 32201−32214

Read Online

ACCESS | Metrics & More | Article Recommendations

ABSTRACT: Genetically engineered fusion polypeptides have been investigated to introduce unique bio-functionality and improve some therapeutic activity for anti-angiogenesis. We report herein that stimuli-responsive, vascular endothelial growth factor receptor 1 (VEGFR1) targeting fusion polypeptides composed of a VEGFR1 (fms-like tyrosine kinase-1 (Flt1)) antagonist, an anti-Flt1 peptide, and a thermally responsive elastin-based polypeptide (EBP) were rationally designed at the genetic level, biosynthesized, and purified by inverse transition cycling to develop potential anti-angiogenic fusion polypeptides to treat neovascular diseases. A series of hydrophilic EBPs with different block lengths were fused with an anti-Flt1 peptide, forming anti-Flt1-EBPs, and the effect of EBP block length on their physicochemical properties was examined. While the anti-Flt1 peptide decreased phase-transition temperatures of anti-Flt1-EBPs, compared with EBP blocks, anti-Flt1-EBPs were soluble under physiological conditions. The anti-Flt1-EBPs dose dependently inhibited the binding of VEGFR1 against vascular endothelial growth factor (VEGF) as well as tube-like network formation of human umbilical vein endothelial cells under VEGF-triggered angiogenesis in vitro because of the specific binding between anti-Flt1-EBPs and VEGFR1. Furthermore, the anti-Flt1-EBPs suppressed laser-induced choroidal neovascularization in a wet age-related macular degeneration mouse model in vivo. Our results indicate that anti-Flt1-EBPs as VEGFR1-targeting fusion polypeptides have great potential for efficacious anti-angiogenesis to treat retinal-, corneal-, and choroidal neovascularization.

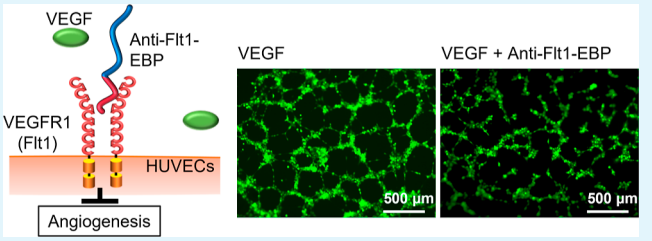

KEYWORDS: *vascular endothelial growth factor receptor 1 targeting peptide, elastin-based polypeptides, stimuli-responsiveness, anti-angiogenesis, neovascular diseases*

INTRODUCTION

Polypeptide-based biomaterials with bio-functionality have been attracting growing interest, with increasing approvals for preclinical and clinical developments.[1,2] Functional peptides and proteins that are capable of specific types of molecular interactions with cells, such as binding, penetration, and membrane disruption, are fused with a variety of polypeptides, forming artificial chimeras or fusion proteins that have multi-functionality for treatment of diseases.[3−6] Artificially designed, multi-functional fusion proteins are engineered by recombinant DNA technologies to precisely control the amino acid sequence and its composition, order of gene combination, molecular weight (MW), hydrophilicity/hydrophobicity, and stimuli responsiveness so that they have biocompatibility with minimal toxicity and immunogenicity and enhanced pharmacokinetics and pharmacodynamics with optimized biodegradation.[7] Generally, a number of fusion proteins are bio-synthesized by prokaryotic and eukaryotic gene expression systems and separated by either conventional column chromatography or inverse transition cycling (ITC) as a non-chromatographic method based on controlled phase transition triggered by their environmental responsiveness.[7,8] For example, antigen-binding variable domains in tumor-targeting antibodies derived from mice by hybridoma technology were genetically fused with human immunoglobulin G (IgG) and shown to decrease immunogenicity in vivo.[9] Antimicrobial peptides in host-defense were combined with the fragments of intracellular protein PurF in *Escherichia coli* (*E. coli*) at the genetic level to overcome several limits including relatively poor stability, short half-life, and high cost of production by bacterial expression.[10] Recently, stimuli-responsive polypeptides which are elastin- or resilin-like biopolymers with unique phase-transition behavior controlled by temperature, pH, and ionic strength were used as fusion proteins to introduce stimuli-triggered dynamic self-assembly and improve the stability of fusion proteins in vivo for advanced drug delivery systems.[11,12]

Received: March 20, 2023
Accepted: June 16, 2023
Published: June 29, 2023

Elastin-based polypeptide (EBP) fusion proteins have been developed for biomedical applications.[13] Elastin as the extracellular matrix protein has elastomeric and crosslinking domains, where the elastomeric ones consist of hydrophobic amino acids as well as repetitive peptides such as VPGG, VPGVG, and APGVGV. EBPs are designed based on the elastomeric domain to have unique stimuli-responsiveness, biocompatibility, biodegradability, and non-immunogenic characteristics.[14] EBPs are thermally responsive biopolymers formed by multimerization of the pentapeptide repeating unit, Val/Ile-Pro-Gly/Ala-X_{aa}-Gly, in which the X_{aa} at the fourth position can be any amino acid except Pro.[12,14,15] EBPs have characteristic lower critical solution temperature (LCST) behaviors depending on various stimuli under physiological conditions, enabling the ITC-based protein purification to be efficient by temperature-induced phase change of the EBPs in a reversible way.[16−18] Importantly, EBPs in a soluble state function as inert macromolecules such as poly(ethylene glycol) (PEG) as well as drug delivery systems either chemically conjugated with drugs or fused with other proteins for therapeutics, regenerative medicine, and tissue engineering.[12,19−21] The unique LCST behavior and inert property of EBPs with minimal non-specific interactions against other proteins and biomolecules allow diverse biological applications.

EBPs were applied as protein purification labels for the cost-effective, non-chromatographic separation method of target proteins in the form of EBP fusion proteins on a large scale. In addition, EBP fusions with therapeutic proteins resulted in increased stability in vivo so that drug retention time in the target area was prolonged.[18,22] For example, EBPs were genetically fused with recombinant human interferon alpha to increase the half-life for cancer treatment or fibroblast growth factor 21 to increase stability of fusion proteins in vivo and lower the cost of production for type 2 diabetes therapy.[22,23] Furthermore, finely tuned thermal sensitivity of EBPs allows targeted drug delivery by local hyperthermia to reduce side effects. EBP fusion proteins with hydrophilic tumor necrosis factor (TNF) receptor type II (TNFRII) as the TNF alpha antagonist were generated to treat peripheral nerve inflammatory diseases; the EBP-TNFRII fusion proteins in a soluble state were injected and then aggregated into particles at the injected area due to the transition of EBPs at physiological temperature, thereby increasing both half-life and targeting efficiency.[24] Recently, EBPs were fused with lacritin as the protein component of human tears to stimulate tear secretion for dry eye disease therapy or the peptide derived from αB crystalline (αBC-P) to cure geographic atrophy derived from an age-related macular degeneration (ARMD) mouse model. Retention of aggregated fusion proteins increased their biological activity in vivo.[25,26] Especially, intravitreally administered αB crystalline peptide-EBP fusion showed therapeutic potential in dispase-induced proliferative vitreoretinopathy in mice.[27] Importantly, controlled EBP length of the EBP fusion proteins largely affects their thermal sensitivity, biosynthesis yield, distribution in organs, and therapeutic efficiency in vivo.[17,28−30] Likewise, EBPs were genetically combined with interleukin-1 receptor antagonist as drug delivery depots to treat osteoarthritis.[31] Two different lengths of EBPs with varied sequences for the identical transition temperature were used to study the effect of EBP length on both association/dissociation rates of the receptor and the ligand. The results showed that EBPs with a longer chain length had lower dissociation rates between them.

Functional peptides and proteins with anti-angiogenesis activity have been of growing interest to treat neovascularization-related diseases like cancer and non-neoplastic diseases.[32] Especially, different strategies of anti-angiogenesis to treat retinal neovascularization were employed to initiate anti-angiogenesis using pigment epithelial-derived factor (PEDF) as an angiogenesis inhibitor or to block angiogenesis by inhibiting vascular endothelial growth factor (VEGF) binding against vascular endothelial growth factor receptor (VEGFR).[33,34] Retinal neovascularization is a pathological process of eye-related non-neoplastic diseases, such as diabetes, prematurity-related retinopathy, and ARMD, leading to blindness. Various anti-angiogenic peptides or proteins have been developed from endogenous anti-angiogenic proteins to treat these diseases. For example, kallikrein-binding protein (KBP) binds with heparin to prevent heparin-mediated activation of VEGF binding to the VEGFRs. Thus, KBP suppresses retinal neovascularization by inhibition of specific binding between VEGF and VEGFR as well as down-regulation of VEGF.[35]

To overcome the drawbacks of endogenous anti-angiogenic proteins such as difficulty in penetrating tissues and high cost of production due to their large MW and complex structures, anti-angiogenic functional peptides were derived from anti-angiogenic proteins.[36] These anti-angiogenic peptide derivatives, including PEDF, PEDF fragments with 34 amino acids, plasminogen, and plasminogen kringle 5, showed anti-angiogenic activity in retinal neovascularization.[37,38] The anti-VEGF monoclonal antibody bevacizumab as a Food and Drug Administration (FDA)-approved angiogenesis inhibitor specifically binds to VEGF so that angiogenesis is inhibited by blocking VEGF binding to its receptors; this inhibitor has been used to treat cancer and neovascular ARMD.[39] As reported,[40] hindering VEGF binding to its receptors inhibits multiple intracellular signaling pathways triggered by VEGFR1 (fms-like tyrosine kinase-1, Flt1), related with angiogenesis, and VEGFR2, mediating proliferation of endothelial cells.

An anti-Flt1 peptide as an Flt1-targeting peptide for anti-angiogenesis strategies was identified from a high throughput screening system, as reported.[41] Especially, the anti-Flt1 peptide, a hexapeptide composed of glycine, asparagine, glutamine, tryptophan, phenylalanine, and isoleucine (GNQWFI), specifically binds to Flt1 as its antagonist, which blocks molecular interactions of Flt1 with not only VEGF but also placental growth factor as Flt1 ligands.[41] Since the amino acid sequence of anti-Flt1 peptide was identified, the anti-Flt1 peptide was utilized for the treatment of angiogenesis-related diseases and tumors by combining it with gold nanoparticles (AuNPs) or biocompatible polymers to improve poor water solubility of the anti-Fltl1 peptide and its half-life in vivo, as reported.[42−48] The anti-Flt1 peptide-AuNP hybrid nanoparticles achieved anti-angiogenesis by cytotoxicity on endothelial cells and inhibited tumor growth by injection into the vein and accumulation in the tumor.[45,48] Recently, hyaluronic acids (HAs) chemically conjugated with a number of anti-Flt1 peptides were self-assembled into micelle structures with genistein as a tyrosine-specific protein kinase inhibitor so that they improved the half-life in vivo.[42,46,47] Likewise, the anti-Flt1 peptide was clicked with 8-amino-3,6-dioxaoctanoic acid to increase stability in vivo, and its anti-angiogenic activity was further enhanced using the anti-Flt1 peptide in D-form to treat extensive angiogenesis in rheumatoid arthritis.[44] When the anti-Flt1 peptide was conjugated with radionuclide and fluorescent 5-carboxytetra-

https://doi.org/10.1021/acsami.3c03989
ACS Appl. Mater. Interfaces 2023, 15, 32201−32214

methylrhodamine, the molecular conjugates were evaluated as dual-modality agents for imaging tumors.[43] While HA- and PEG-anti-Flt1 conjugates increased its half-life in vivo, its conjugation efficiency and nanostructures were heterogeneous due to polydisperse MW of HA and PEG, broad size distribution of nanostructures, and inconsistent conjugation efficiency of the anti-Flt1 peptide.[44,47] To overcome these limitations, genetically engineered anti-Flt1 fusion proteins need to be developed for therapeutic applications toward anti-angiogenesis.

In this work, we report a series of genetically encoded, stimuli-responsive VEGFR1-targeting fusion polypeptides consisting of both an anti-Flt1 hexapeptide composed of GNQWFI and an EBP block with controlled chain length. We explored their anti-angiogenesis activity against choroidal neovascularization (CNV) in an ARMD mouse model. Laser-induced CNV is derived from lesions such as retinal pigment epithelium detachment and formation of fibrovascular tissue around CNV that damages the vision of ARMD patients.[49] We hypothesized that these anti-Flt1-EBPs as soluble unimers under physiological conditions would have specific noncovalent interactions with VEGFR1 and inhibit tube-like network formation of human umbilical vein endothelial cells (HUVECs) under VEGF-triggered angiogenesis in vitro. The anti-Flt1-EBPs were engineered at the DNA level, highly expressed in bacteria, and non-chromatographically separated based on a thermally responsive EBP block. The anti-Flt1-EBPs as soluble unimers inhibited specific binding between VEGFR1 and VEGF depending on EBP length, representing that they largely suppressed tube-like network formation of HUVECs on the Matrigel substrate. Furthermore, they decreased the lesion sizes of the laser-induced CNV mice models after intravitreal injection (IVT). It clearly indicates that they showed anti-neovascularization in vitro and in vivo. Thus, these genetically engineered anti-Flt1-EBP fusion polypeptides could overcome the limitations that both chemically synthesized peptide-based biomaterials and peptide-polymer conjugates have for biomedical applications in vivo: (1) time and cost-consuming chemical synthesis, conjugation, and purification, (2) polydisperse MWs of polymers, and (3) inconsistent conjugation efficiency and difficulty in selective conjugation. This work suggests that the anti-Flt1-EBPs as VEGFR1-targeting fusion polypeptides with anti-angiogenesis activity would be of great potential to treat neovascularization-related diseases in retina, cornea, and choroid.

EXPERIMENTAL SECTION

Materials. Both pET-21a (+) and BL21 (DE3) *E. coli* strain were provided by Novagen (Madison, WI, USA) and competent *E. coli* Top10 cells by Invitrogen (Carlsbad, CA, USA). Chemically synthesized, single-stranded oligonucleotides were supplied by Cosmogenetech (Seoul, ROK). Restriction enzymes of AcuI, BseRI, BamHI, XbaI, and alkaline phosphatase were obtained from New England Biolabs (Ipswich, MA, USA) and Fermentas (Ontario, Canada) and T4 DNA ligase from Elpis-biotech (Daejeon, ROK). The kits for PCR purification, DNA mini-preparation, and gel extraction were bought from Geneall Biotechnology (Seoul, ROK) and Dyne Agarose High from Dyne Bio (Seongnam, ROK). TB- and Circlegrow (CG) medium were purchased from Mo Bio Laboratories (Carlsbad. CA, USA) and MP Biomedicals (Solon, OH, USA) to grow Top10 and BL21(DE3) cells, respectively. Isopropyl-β-D-thiogalactoside (IPTG) was supplied from Goldbio (Saint Louis, MO, USA). Precast gels were provided from Bio-Rad (Hercules, CA, USA). Polyethyleneimine, bovine serum albumin (BSA), and phosphate buffered saline (PBS) were obtained from Sigma-Aldrich (St. Louis, MO, USA). Recombinant human VEGF-165 ($rhVEGF_{165}$) and VEGFR1 (Flt1)-F_c of IgG (Flt1-F_c) fusion protein were bought from R&D System (Minneapolis, MN, USA) and rabbit anti-human IgG F_c-horseradish peroxidase (HRP) and 3,3′,5,5′-tetramethylbenzidine (TMB) from ThermoFisher Scientific (Waltham, MA, USA). The HUVECs were supplied by American Type Culture Collection (ATCC) (Manassas, VA, USA) and the growth medium by PromoCell (Heidelberg, Germany). HUVECs at passages from 6 to 8 were used. Endothelial basal medium-2 (EBM-2) and endothelial growth medium-2 bullet kits were obtained from Lonza (Basel, Switzerland). The viability of HUVECs was quantified by a cell counting kit-8 (CCK-8) from Dojindo Laboratories (Kumamoto, Japan). Calcein-AM was purchased from Invitrogen (Carlsbad, CA, USA) and Matrigel from BD Biosciences (San Diego, CA, USA). Bevacizumab was sourced from Roche Pharma (Reinach, Switzerland), aflibercept from Ichorbio (Oxford, UK), ketamine from Huons (Seongnam, ROK), xylazine from Bayer (Leverkusen, Germany), and tropicamide from Santen Pharmaceutical (Kita-ku, Osaka, Japan). Formalin and fluorescein isothiocyanate (FITC)-dextran (MW 2000 kDa) were obtained from Sigma-Aldrich (St Louis, MO, USA).

Gene Assembly of EBP*n* and Anti-Flt1-EBP*n* Fusion Polypeptides. The modified pET-21a (+) (mpET-21a) vector with an adaptor DNA sequence was prepared, as previously reported.[50,51] The adaptor of mpET-21a has the identical cleavage site of BseRI and AcuI and leaves two different sticky ends of XbaI and BamHI for seamless ligation of EBP*n* and anti-Flt1-EBP*n* encoded genes. EBP*n* with the pentapeptide unit of Val-Pro-Ala-X_{aa}-Gly (VPAXG), where X at the fourth residue is an amino acid except Pro, is composed of *n* integer repeats of the six pentapeptides with the X composition of Ala:Gly:Ile of 1:4:1. A pair of oligonucleotide cassettes to encode the anti-Flt1 peptide or EBP1 with cohesive ends of both BseRI and AcuI were annealed by heating oligonucleotide solutions at 95 °C and slowly cooling them to room temperature. The linearized mpET-21a, which was restricted and dephosphorylated by 15 U BseRI and alkaline phosphatase, was ligated with the annealed DNA encoding EBP1 by incubating 30 pmol mpET-21a with 90 pmol EBP1 gene in the presence of 1 U T4 DNA ligase. The ligates of both mpET-21a and EBP1 were transformed into the competent Top10 cells, followed by incubating the transformants on the SOC plates with 50 μg/mL ampicillin. They were screened to determine a length of EBP1 gene by agarose gel electrophoresis with double digestion of XbaI and BamHI and confirmed by DNA sequencing. When a series of genes of EBP*n* (n = 1−6) were constructed, EBP12 and EBP24 were prepared by serial multimerization of EBP6 gene by modified recursive directional ligation (RDL), as reported.[7,50,51] Likewise, to construct various genes encoding anti-Flt1-EBP*n* (n = 3, 6, 12, 24), 90 pmol annealed anti-Flt1 peptide-encoded dsDNA with both BseRI and AcuI cohesive ends was incubated with 30 pmol BseRI-restricted EBP*n*-encoding mpET-21a vector using 1 U T4 DNA ligase for ligation. Both gene and its length of anti-Flt1 peptide and EBP*n* were confirmed with XbaI and BamHI digestion by agarose gel electrophoresis and DNA sequencing.

Expression and Non-chromatographic Separation of EBP*n* and Anti-Flt1-EBP*n*. BL21(DE3) cells transformed with the respective mpET-21a vector containing EBP*n* or anti-Flt1-EBP*n* were grown overnight in 50 mL of the CG medium with 50 μg/mL ampicillin at 37 °C and 200 rpm. Then, 50 mL of the starter-culture solution was injected in 500 mL of the CG medium with 50 μg/mL ampicillin and incubated on a shaking incubator at 37 °C and 200 rpm for 16 h. When the culture reached an optical density at 600 nm of 1.0, over-expression of EBP*n* or anti-Flt1-EBP*n* was induced by adding IPTG at a final concentration of 1 mM. To non-chromatographically purify EBP*n* or anti-Flt1-EBP*n*, the *E. coli* cells were separated by centrifugation at 4500 rpm for 10 min at 4 °C and LCST-based ITC was executed, as reported.[18,50,51] In brief, the cells resuspended in 30 mL of PBS were lysed on ice by ultra-sonication with intervals of 10 s on and 20 s off for 5 min (VC-505, Sonic and Materials, Danbury, CT, USA), followed by centrifugation at 13 000

https://doi.org/10.1021/acsami.3c03989
ACS Appl. Mater. Interfaces 2023, 15, 32201−32214

rpm for 15 min at 4 °C. When the insoluble cell debris was precipitated, the supernatant with soluble EBP*n* or anti-Flt1-EBP*n* was mixed with polyethyleneimine (0.5% w/v), and the mixture solution was centrifuged under identical conditions to precipitate the nucleic acids. The phase transition of both EBP*n* and anti-Flt1-EBP*n* from a soluble to an insoluble state was induced with 3 M NaCl, and the aggregates were then separated at 40 °C by centrifugation at 13 000 rpm for 15 min. The pellets were suspended in PBS on ice and then centrifuged at 4 °C to precipitate irreversibly aggregated contaminants. Likewise, one cycle of ITC for aggregation and resuspension was repeated 5−10 times depending on EBP chain length and anti-Flt1 peptide fusion.

Characterization of EBP*n* and Anti-Flt1-EBP*n*. Both MWs and purities of EBP*n* and anti-Flt1-EBP*n* were determined by calculating the relative migration distances of SDS-PAGE with copper staining and gel filtration chromatography (high-performance liquid chromatography 1260, Agilent, Palo Alto, CA, USA) with a Bio-Rad ENrich GFC 70 10 × 300 column (Bio-Rad Laboratories, CA, USA). The filtered solution of EBP*n* and anti-Flt1-EBP*n* was eluted in deionized water at 1.0 mL/min and monitored by measuring the absorbance at 280 nm. The effect of temperature on LCST behavior of 25 μM EBP*n* and anti-Flt1-EBP*n* in PBS with 0−2 M NaCl was determined by measuring the optical density at 350 nm on a Cary 100 Bio UV/Vis spectrophotometer equipped with a thermoelectric temperature controller of multi-cells (Varian, Walnut Creek, CA, USA), which controlled the temperature in the range from 10 to 85 °C at 1.0 °C/min for heating.

Binding of Anti-Flt1-EBP*n* against Flt1. Binding of anti-Flt1-EBP*n* against Flt1 in PBS was examined by indirect enzyme-linked immunosorbent assay (ELISA), as reported elsewhere.[41,46] First, $rhVEGF_{165}$ (MW 38.4 kDa) in a homo-dimeric form at 500 ng/mL was incubated in each well of a 96-well plate at 4 °C overnight for its surface-coating, followed by washing it with 0.05 w/v % Tween-20 in PBS to completely remove uncoated $rhVEGF_{165}$. In addition, 3 w/v % BSA in PBS in each well was incubated at room temperature for 2 h to block unoccupied sites on the $rhVEGF_{165}$-coated surface, and the unbound BSA was removed with 0.05 w/v % Tween-20 in PBS. Second, the human Flt1-F_c fusion protein (MW 200.0 kDa) in a homodimer at 0.5 μg/mL was separately incubated in PBS with 1 w/v % BSA and anti-Flt1-EBP*n* at different concentrations in the range of 0.5−500 μM for 2 h to have specific binding between anti-Flt1 peptide and Flt1, followed by adding each solution to the $rhVEGF_{165}$-coated wells and incubating it for 2 h at ambient temperature. EBP12 under identical conditions was used as control. Each well was washed with 0.05 w/v % Tween-20 in PBS to remove unbound Flt1-F_c proteins. Finally, human Flt1-F_c protein bound to the $rhVEGF_{165}$-coated well was incubated with rabbit anti-human IgG F_c-HRP conjugate in PBS with 0.3 w/v % BSA for 1 h, and each well was then washed eight times with 0.05 w/v % Tween-20 in PBS. TMB as a chromogenic substrate of HRP was added to each well, and the oxidized TMB was quantified by measuring the absorbance at 450 nm. Each experiment in indirect ELISA was executed three times to confirm reproducibility.

Cytotoxicity of Anti-Flt1-EBP*n* on HUVECs. The viability of HUVECs treated with EBP12 or anti-Flt1-EBP*n* was quantified by water-soluble tetrazolium salt (WST-8) of CCK-8. The HUVECs at 3 × 10^3 cells/well were placed in triplicate in the 98-well plate, incubated overnight, and treated with 100 μL of 0.1, 1, 10, and 100 μM EBP12 and anti-Flt1-EBP*n* in EBM-2 at 37 °C for 24 and 48 h. Then, the media containing EBP12 and anti-Flt1-EBP*n* were replaced with 100 μL of EBM-2 containing 10% WST-8. Color change of the medium was measured by absorbance at 450 nm when incubated for 4 h.

Inhibition of Anti-Flt1-EBP*n* on Tube-like Network Formation of HUVECs. To evaluate the biological activity of soluble anti-Flt1-EBP*n*, VEGF-induced HUVEC tube-like network formation assay was performed. Each well of 48-well cell culture plates was surface-coated by incubating 200 μL of 8.7 mg/mL Matrigel at 37 °C for 1 h. HUVECs were stained with 10 μM calcein-AM as a cell permeant fluorescence dye at 37 °C for 15 min and then washed with PBS repeatedly. Calcein-labeled HUVECs (2 × 10^4 cells per well) seeded on Matrigel with $rhVEGF_{165}$ at 50 ng/mL were separately treated with EBP12 or anti-Flt1-EBP*n* at different concentrations (0.1−10 μM) at 37 °C for 4 h. Bevacizumab, a humanized monoclonal antibody against VEGF in the concentration range of 8 to 200 μg/mL was investigated as a positive control. The HUVECs were imaged under the micromanipulator (Olympus, Tokyo, Japan) and quantitatively analyzed by calculating the whole length of their tube-like networks in three randomly selected, different fields of each well with Image Lab (Bio-Rad, Hercules, CA, USA).

Anti-neovascularization of Anti-Flt1-EBP12 in the Laser-Induced CNV Model. Six- to eight-week-old female C57BL-6 mice of wild-type were provided by Orient Bio (Sungnam, ROK). Laser injury of Bruch's membrane in the C57BL-6 mice induced CNV, as reported.[49] Four or five 532 nm diode laser spots under the conditions of 210 mW and 100 μm (OcuLight TX and IQ 532, Iridex, Mountain View, CA, USA) were given for 0.1 s to each fundus by means of a coverslip. IVT was executed once immediately after laser injury under a stereomicroscope, OAM 24 NS (Dongwon, Bucheon, ROK). Soluble anti-Flt1-EBP12 (5 and 10 μg), EBP12 (10 μg), PBS (2 μL) as the control, and aflibercept (1 and 10 μg) as the positive control were separately injected into the vitreous spaces of the eyes at a flow rate of 200 nL/s by a micro-syringe pump controller, Micro4 (World Precision Instruments, Sarasota, FL, USA). Sizes of CNV lesions were analyzed using whole flat mounts of retina on day 14 after laser injury, as reported.[52] Retro-orbital injection of FITC-dextran at 25 mg/mL was performed under anesthesia. Enucleation of the eyes was executed, followed by fixation with 10% formalin for 30 min. Each of the cornea, iris, lens, and vitreous was separated under a stereomicroscope (Leica, Wetzlar, Germany). Four different radial incisions in the dissected retina were performed, and it was then flattened by the coverslip. The CNV lesions were imaged by a fluorescence microscope with a magnification of ×200. The sizes of CNV lesions were measured automatically when the outer boundary of the CNV lesion was marked with a line in the image of the NanoZoomer 2.0 RS software. (Hamamatsu Photonics, Hamamatsu, Japan).

Systemic Toxicity of Anti-Flt1-EBP12 in Mice. Soluble anti-Flt1-EBP12 (1 and 10 mg/kg) and PBS as the control were administered once as an intraperitoneal injection at a volume of 100 μL to six-week-old female C57BL-6 mice. Then, the effect of anti-Flt1-EBP12 on the mouse was observed for one week, the death of the mouse was observed, and the weight was measured; the changes in appearance and behavior were evaluated every day.

Statistical Analysis. Data are represented as the mean and standard deviation (SD). All statistical analyses were executed using the Prism software (GraphPad, San Diego, CA, USA). Comparison of means was performed by an unpaired *t*-test or Dunnett's multiple range test. $p < 0.05$ was determined to be statistically significant.

RESULTS AND DISCUSSION

We generated anti-Flt1-EBP*n* fusion polypeptides with four different lengths of the EBP block to optimize EBP chain length for anti-angiogenesis. Figure 1A shows the genes encoding the anti-Flt1 peptide and EBP repeating unit, their amino acid sequences, and a schematic of anti-Flt1-EBP*n* fusion polypeptides. The anti-Flt1 peptide, GNQWFI, was introduced for its specific binding to VEGFR1 (Flt1) as an antagonist, while the thermally responsive EBP block without any charged amino acid residues was designed as the hydrophilic block to make the transition temperature (T_t) higher than the body temperature. $EBP[A_1G_4I_1]_n$ is defined as follows: (1) The capital letters in the bracket indicate symbols of amino acids located at the fourth position of the repetitive pentapeptide unit, VPAXG. (2) Their subscripts show ratios of the X amino acids of the pentapeptide repeats. (3) Finally, the *n* integer represents the number of the six pentapeptide repeats, which is designated as EBP*n* (n = 1, 3, 6, 12 and 24).

https://doi.org/10.1021/acsami.3c03989
ACS Appl. Mater. Interfaces 2023, 15, 32201−32214

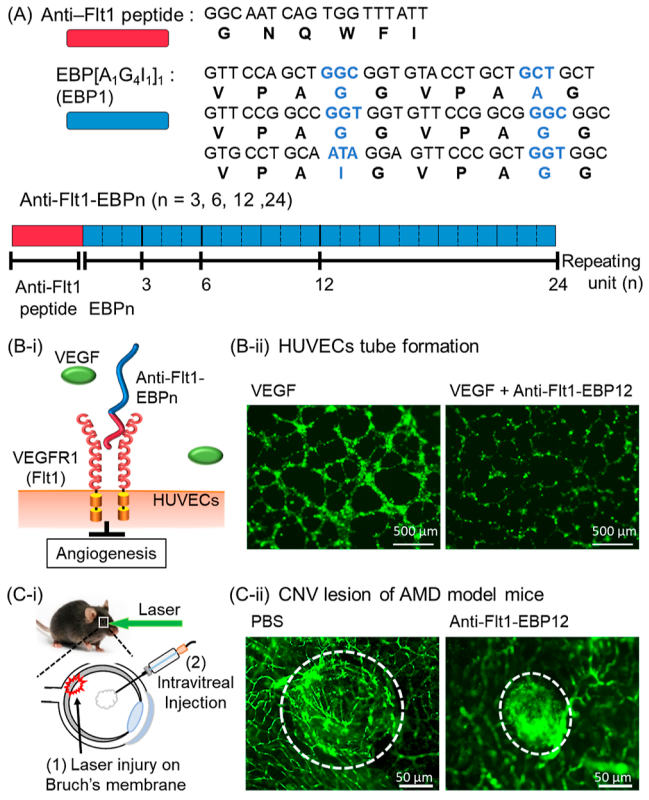

Figure 1. (A) Genes encoding anti-Flt1 peptide and EBP$[A_1G_4I_1]_1$ (EBP1) repeating unit and their amino acid sequences are shown on the top. A schematic of anti-Flt1-EBP*n* fusion polypeptides with four different lengths of the EBP block (n = 3, 6, 12, and 24) is shown at the bottom. (B) Schematic of the anti-angiogenesis molecular mechanism of anti-Flt1-EBP*n* (B-i) and images of tube-like network formation of HUVECs labeled with calcein-AM by fluorescence microscopy when they were incubated with VEGF only as control (left) and anti-Flt1-EBP12 with VEGF (right) (B-ii). (C) Cartoon showing how to prepare the CNV mouse model using laser and perform IVT of anti-Flt1-EBP12 (C-i) and fluorescence microscopic images of the FITC-dextran-stained CNV lesions (white dotted circles) of the wet ARMD mouse injected with PBS as control (left) and anti-Flt1-EBP12 after laser-induced injury (right). Scale bars are 500 μm in (B-ii) and 50 μm in (C-ii).

Especially, to ensure high T_t of EBP*n* under physiological conditions, both ratio and order of the three different amino acids, A, G, and I, at the fourth amino acid of the pentapeptide units of EBP1 were optimized as compared with the T_ts of EBPs in the previous reports.[7,14,53]

Figure 1B represents a schematic with the potential anti-angiogenesis mechanism of the anti-Flt1-EBP fusion polypeptides (i) and fluorescence microscopic images of HUVECs labeled with calcein-AM (ii) when they were incubated with either VEGF as the control or VEGF with anti-Flt1-EBP12. We hypothesized that anti-Flt1-EBPs as Flt1-targeting fusion polypeptides could bind Flt1 via specific non-covalent interactions in the presence of VEGF, blocking the interaction of Flt1 with VEGF to prevent angiogenesis. The thermally sensitive, hydrophilic EBP block at the C-terminal was introduced as a non-chromatographic purification polypeptide tag so that it could be purified using thermally triggered aggregation of the anti-Flt1-EBPs with reversibility. While the anti-Flt1 peptide has poor solubility in water,[41,45−48] hydrophilicity of the EBP block with the T_t higher than the body temperature makes anti-Flt1-EBP*n* completely soluble under physiological conditions, which would avoid any hindrance to the anti-angiogenic effect of the anti-Flt1 peptide due to aggregation. Furthermore, the EBP block of the bioactive fusion polypeptides would show minimal non-specific binding with other biomolecules and increased half-life in vivo because of its inert characteristics such as PEG-conjugates, as reported.[31,54] When HUVECs were treated with VEGF and anti-Flt1-EBP12, tube-like network formation of HUVECs was dramatically inhibited compared with that of the VEGF-treated HUVECs as control. We further explored whether anti-Flt1-EBP12 could inhibit CNV in a wet ARMD mouse model in vivo; a schematic of the laser-induced CNV model and injection of anti-Flt1-EBP12 into the vitreous is shown in Figure 1C-i. A laser at 532 nm wavelength was pointed against the Bruch's membrane of the choroid (the vascular layer between sclera and retina of the eye) for its collapse to induce the CNV model of retinal neovascular disease such as wet ARMD, as reported.[49] Figure 1C-ii represents that the FITC-dextran stained CNV lesions of mice injected with anti-Flt1-EBP12 were largely suppressed, while PBS-treated control mice showed progression of CNV lesions.[49] These results indicate that anti-Flt1-EBP fusion polypeptides inhibited VEGF-induced tube-like network formation of HUVECs in vitro and decreased sizes of CNV lesions in vivo.

The genes of the hydrophilic EBP block, EBP*n* and the anti-Flt1-EBP*n* fusion polypeptides, were constructed by a unique molecular cloning methodology.[7] As shown in Figure 2A, the adaptor DNA sequence, which has the identical restriction site of both BseRI and AcuI as well as two different cohesive ends of XbaI and BamHI, was introduced to the linearized pET-21a (+) plasmid for unique seamless ligation, forming the modified pET-21a (+) (mpET-21a). Both BseRI-restricted mpET-21a and EBP1 gene were ligated, and the EBP1 gene was then multimerized to construct a series of EBP*n* (n = 3, 6, 12, and 24) via modified RDL, as described.[7] For example, to prepare the EBP12-encoding plasmid, the plasmid containing EBP6 was digested with XbaI and AcuI, which flank the EBP6 gene. The EBP6 gene fragment was then ligated with the vector containing EBP6 that was digested with XbaI and BseRI. Likewise, the genes encoding anti-Flt1-EBP*n* were constructed by insertion of the chemically synthesized and annealed DNA fragment encoding anti-Flt1 peptide into the BseRI-digested EBP*n* vector. Figure 2B,C shows photographic images of agarose gel electrophoresis of EBP*n* and anti-Flt1-EBP*n*-encoded genes when they were digested with both XbaI and BamHI. The lengths of digested DNAs encoding EBP*n* were 336, 606, 1146, and 2226 base pairs, while those of anti-Flt1-EBP*n* were 354, 624, 1164, and 2244 base pairs. Their DNA lengths are shown to be 66 base pairs longer than the gene sizes because the restriction sites of XbaI and BamHI are located in the regions flanking EBP*n* and anti-Flt1-EBP*n* (Table 1). Importantly, XbaI and BamHI were used instead of BseRI and AcuI placed at both ends of the genes encoding EBP*n* and anti-Flt1-EBP*n* because the mpET-21a vector has three restriction sites of AcuI and the DNA sizes of mpET-21a restricted with AcuI are 943, 1012, and 3477 base pairs, which would overlap with the sizes of genes encoding EBP*n* and anti-Flt1-EBP*n*. Furthermore, the gene length of anti-Flt1-EBP*n* is 18 bp longer than that of EBP*n* because the gene encoding the anti-Flt1-EBP*n* was constructed via seamless ligation, as confirmed by DNA sequencing.

https://doi.org/10.1021/acsami.3c03989
ACS Appl. Mater. Interfaces 2023, 15, 32201−32214

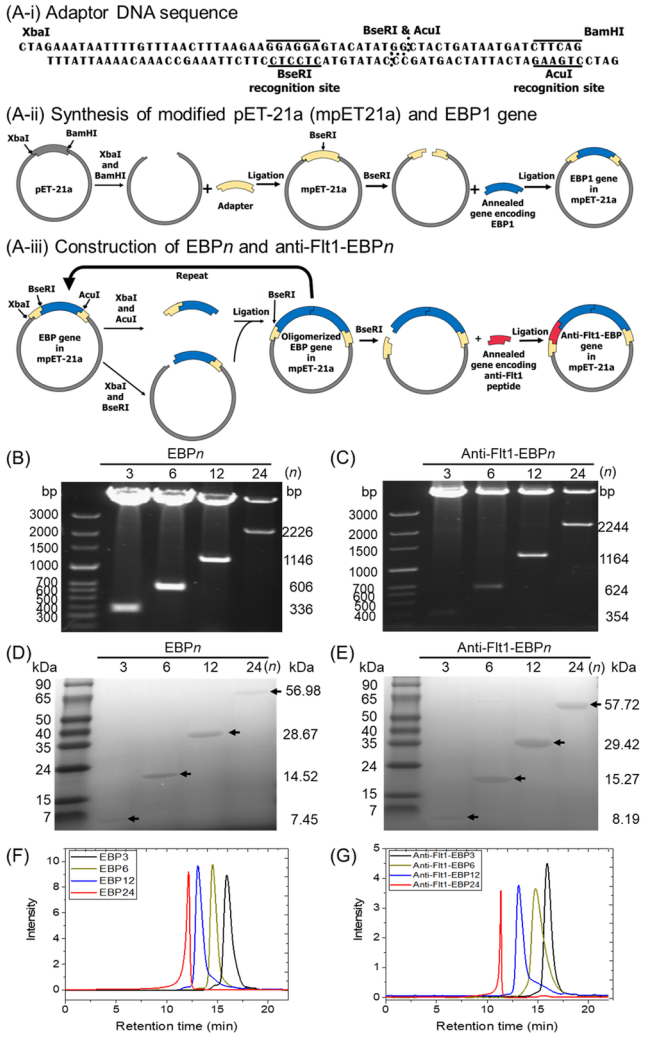

Figure 2. (A) Adaptor DNA sequence with the identical restriction site of both BseRI and AcuI as well as two different sticky ends of XbaI and BamHI for pET-21a (+) modification (i), schematic of insertion of the adaptor sequence into the linearized pET-21a (+) plasmid to generate the modified pET-21a (+) (mpET-21a) and integration of the EBP1 gene into the mpET-21a vector restricted with BseRI to generate the plasmid encoding EBP1 (ii), and overview of multimerization of EBP1 by using RDL methodology to construct EBP*n* (n = 3, 6, 12, and 24) and introduction of the chemically synthesized and annealed DNA fragment encoding anti-Flt1 peptide into the BseRI-digested EBP*n* vector to have genes encoding anti-Flt1-EBP*n* (iii). (B,C) Photographic agarose gel images of the constructed genes encoding (B) EBP*n* and (C) anti-Flt1-EBP*n* (n = 3, 6, 12, and 24) by electrophoresis. DNA size markers are labeled on the left of the gel and DNA lengths of EBP*n* and anti-Flt1-EBP*n* are indicated on the right of the gel. (D,E) Copper-stained gel images of SDS-PAGE of (D) EBP*n* and (E) anti-Flt1-EBP*n* (n = 3, 6, 12, and 24). The bands of EBP*n* and anti-Flt1-EBP*n* in the SDS-PAGE gels are indicated by the arrows. Protein markers are shown on the left of the gel, and the expected MWs of EBP*n* and anti-Flt1-EBP*n* are indicated on the right of the gel in (D,E). The MWs of EBP*n* are 7.45, 14.52, 28.67, and 56.98 kDa while those of anti-Flt1-EBP*n* are 8.19, 15.27, 29.42, and 57.72 kDa. The MW of anti-Flt1-EBP*n* is 763.84 Da larger than that of EBP*n* under the identical EBP length due to the hexapeptide of anti-Flt1 peptide, GNQWFI. (F,G) SEC profiles of (F) EBP*n* and (G) anti-Flt1-EBP*n* (n = 3, 6, 12 and 24) by UV absorbance.

Table 1. Gene Lengths and MWs of EBP*n* and anti-Flt1-EBP*n* and Their T_ts in 10 mM PBS Supplemented with 0−2 M NaCl and the Degree of Temperature Decrease after Fusion with anti-Flt1 Peptide[a]

			transition temperatures (T_ts)		
library	nucleotide chain length (bp)	MW (kDa)	0 M NaCl	1 M NaCl	2 M NaCl
EBP3	270	7.45	N/A	N/A	57.12
EBP6	540	14.52	N/A	74.07	50.22
EBP12	1080	28.67	75.37	50.35	33.12
EBP24	2160	56.98	62.52	42.47	27.42
Anti-Flt1-EBP3 ($^b\Delta T_t$)	288	8.19	N/A	N/A	N/A
Anti-Flt1-EBP6 ($^b\Delta T_t$)	558	15.27	N/A	60.07 (14.00)	36.02 (14.20)
Anti-Flt1-EBP12 ($^b\Delta T_t$)	1098	29.42	66.12 (9.25)	44.07 (6.28)	26.12 (7.00)
Anti-Flt1-EBP24 ($^b\Delta T_t$)	2178	57.72	57.22 (8.30)	38.27 (4.23)	23.47 (3.95)

[a]The T_t values were determined by measuring an inflection point of the thermal profiles of Figure 3. [b]ΔT_t is the difference in T_t when anti-Flt1 peptide was fused to EBP*n* (n = 3, 6, 12, and 24) in PBS supplemented with 0−2 M NaCl.

Temperature-responsive EBP*n* and anti-Flt1-EBP*n* with controlled EBP length were synthesized in *E. coli* and separated non-chromatographically to investigate the effect of anti-Flt1 peptide fusion on physicochemical properties. The yields of EBP*n* and anti-Flt1-EBP*n* were 1−10 mg/L and 3−50 mg/L, respectively, depending on EBP length and anti-Flt1 peptide fusion. Generally, the yield increased as the EBP length increased. Introduction of anti-Flt1 peptide at the N-terminal increased the yield, which is matched with the previous study that proteins fused at the N-terminal of EBP block increased the yield of fusion proteins.[55] Photographic images of copper-stained SDS-PAGE gels of EBP*n* and anti-Flt1-EBP*n* in Figure 2D,E show a single protein band per lane, indicating high purity by ITC purification. The theoretical MWs of EBP*n* are 7.45, 14.52, 28.67, and 56.98 kDa, while those of anti-Flt1-EBP*n* are 8.19, 15.27, 29.42, and 57.72 kDa. The MW of anti-Flt1-EBP*n* is 763.84 Da larger than that of EBP*n* under identical EBP length due to the hexapeptide of anti-Flt1 peptide, GNQWFI. The apparent MWs of EBP*n* and anti-Flt1-EBP*n* were determined by their relative migration distances as presented in Figure 2D,E. Importantly, the apparent MWs of EBP*n* are 7.26, 16.26, 31.76, and 61.58 kDa, while those of anti-Flt1-EBP*n* are 9.17, 17.99, 32.86, and 68.92 kDa which are 0.06−19.41% closer to their expected MWs, as reported.[7,56] Furthermore, the purity of EBP*n* and anti-Flt1-EBP*n* was determined by size exclusion chromatography (SEC) equipped with an ultraviolet detector. The retention times (R_ts) of EBP*n* were 15.95, 14.54, 13.09, and 12.16 min, while those of anti-Flt1-EBP*n* were 15.93, 14.79, 13.12, and 11.71 min in the SEC traces of Figure 2F,G. Each sharp single peak per SEC trace indicated that the purity of the EBP*n* was in the range of 98.3−99.8% while that of anti-Flt1-EBP*n* was in the range of 97.2−99.8%. The anti-Flt1 peptide at N-terminal of anti-Flt1-EBP*n* had no significant interactions with impurities during ITC purification. In addition, the R_t of anti-Flt1 EBP*n* showed no

https://doi.org/10.1021/acsami.3c03989
ACS Appl. Mater. Interfaces 2023, 15, 32201−32214

significant difference with that of EBP*n* under the identical EBP length because of the hexapeptide of anti-Flt1.

The thermal transition behavior of EBP*n* and anti-Flt1-EBP*n* was investigated to study the effects of anti-Flt1 peptide fusion, EBP block length, and NaCl concentration on the transition temperature (T_t). Figure 3 shows the turbidity profiles of EBP*n* and anti-Flt1-EBP*n* at 25 μM in 10 mM PBS supplemented with 0−2 M NaCl. The turbidity profiles were obtained by measuring absorbance at 350 nm in which insoluble proteins show apparent absorption without intrinsic absorbance of proteins.[57,58] The T_t was determined from a point of inflection of each thermal profile and are summarized in Table 1. As shown in Figure 3A, both EBP*n* and anti-Flt1-EBP*n* in PBS showed T_ts higher than 55 °C. This indicates that under physiological conditions (below the T_t), EBP*n* and anti-Flt1-EBP*n* were completely soluble due to the hydrophilic characteristics of EBP*n*, which would allow specific binding of anti-Flt1-EBP*n* to VEGFR1 without any steric hindrance. The T_ts of anti-Flt1-EBP*n* with 12 and 24 repeating units in PBS were approximately 9.25 and 8.30 °C lower than those of EBP*n* under the identical EBP length because the hydrophobicity of GNQWFI of the anti-Flt1 peptide for VEGFR1 targeting largely decreased the T_ts of anti-Flt1-EBP*n*. Although the EBP*n* and anti-Flt1-EBP*n* with the repeating units of 12 and 24 in PBS only showed thermally triggered aggregation below 90 °C, the T_ts became lower as the EBP block length increased, irrespective of anti-Flt1 peptide fusion, which is matched with previously reported EBP fusion proteins.[7,58] In addition, to characterize the temperature-induced transition behavior of EBP*n* and anti-Flt1-EBP*n* with repeating units of 3 and 6, the T_ts of EBP*n* and anti-Flt1-EBP*n* were measured by preparing PBS supplemented with 1−2 M NaCl, as increased salt concentration decreased T_ts of EBPs and EBP fusions.[58] Figure 3B,C shows that all of the EBP*n* and anti-Flt1-EBP*n* exhibited phase transition in PBS with 1 M NaCl (B) and 2 M NaCl (C). The T_ts of anti-Flt1-EBP*n* with the repeating units of 6, 12, and 24 in PBS with 1 M NaCl were approximately 14.00, 6.28, and 4.23 °C lower than those of EBP*n* with the corresponding EBP length, respectively. Likewise, the T_ts of anti-Flt1-EBP*n* with the repeating units of 6, 12, and 24 in PBS with 2 M NaCl were approximately 14.20, 7.00, and 3.95 °C lower than those of the respective EBP*n*, respectively. Because of the hydrophobicity of anti-Flt1 peptide, the T_t of the anti-Flt1-EBP*n* largely decreased irrespective of NaCl concentration as the EBP block length became shorter, which is shown in Figure 3D. In addition, the T_ts of EBP*n* and anti-Flt1-EBP*n* largely decreased as both EBP length and NaCl concentration increased, facilitating non-chromatographic purification with high purity for therapeutic applications.[7,58] It was reported that LCST behavior and T_t of EBP were reproducible under identical conditions such as buffer composition, pH, protein concentration, and heating rate.[7,58] The T_ts of EBP*n* and anti-Flt1-EBP*n* in Figure 3 were identical in the repeated measurements (data not shown).

Figure 4A represents a cartoon of competitive and indirect ELISA to evaluate the effect of anti-Flt1-EBP*n* on the inhibition of the interaction of Flt1 and rhVEGF$_{165}$. With the absorbance value in Flt1-F$_c$ binding on the rhVEGF$_{165}$-coated well in the absence of EBP12 or anti-Flt1-EBP*n* considered as 100% binding, the percentage of inhibition was calculated (Figure 4B). There was no significant inhibition of EBP12 on the binding of Flt1-F$_c$ and rhVEGF$_{165}$ irrespective of different concentrations. Anti-Flt1-EBP*n* markedly inhibited binding

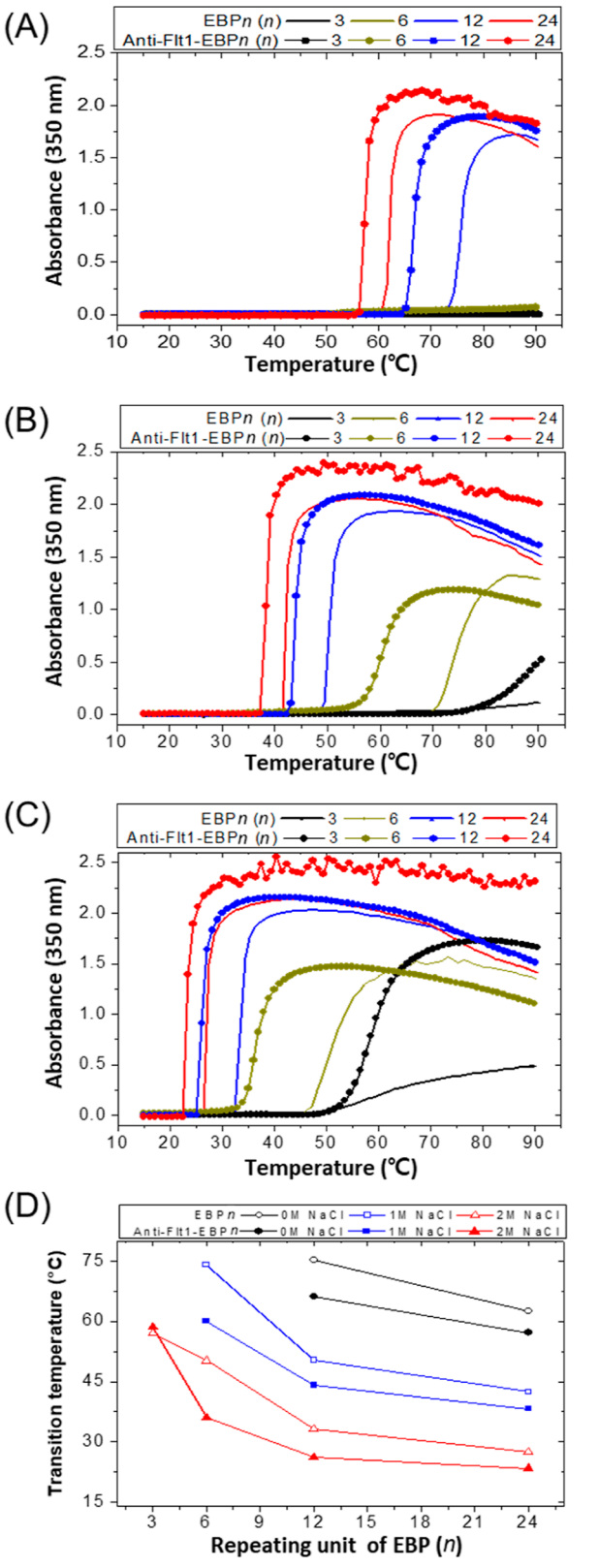

Figure 3. (A−C) Temperature-dependent turbidity profiles of both EBP*n* and anti-Flt1-EBP*n* at 25 μM in PBS (A), PBS supplemented with different salt concentrations, 1.0 M NaCl (B) and 2.0 M NaCl (C), by calculating the absorbance at 350 nm under the condition of 1 °C/min for heating. (D) Plots of NaCl concentration-dependent transition temperatures based on the EBP repeating number.

https://doi.org/10.1021/acsami.3c03989
ACS Appl. Mater. Interfaces 2023, 15, 32201−32214

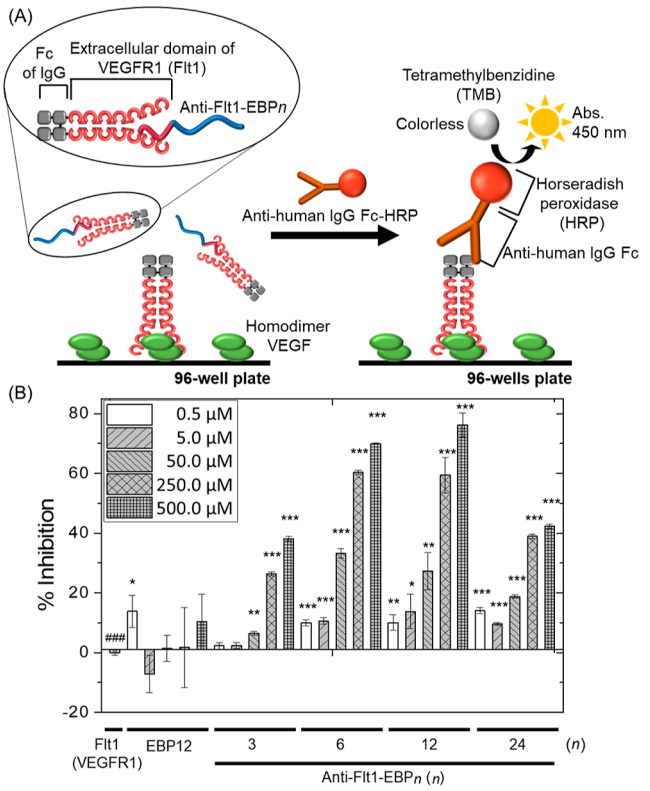

Figure 4. (A) Schematics of the mechanism of anti-Flt1-EBP*n* to inhibit binding of VEGFR1 (Flt1) to recombinant human VEGF165 ($rhVEGF_{165}$), as characterized by the indirect ELISA. The recombinant human Flt1-F_c of IgG_1 chimeric protein (Flt1-F_c) was separately incubated with the EBP12 as control and anti-Flt1-EBP*n* at different concentrations, followed by its addition to $rhVEGF_{165}$-coated wells and incubation. The Flt1-F_c bound with anti-Flt1-EBP*n* was removed by washing in PBS. The Flt1-F_c bound to the $rhVEGF_{165}$ on the well was quantified by incubation with the molecular conjugate of anti-human IgG F_c-HRP and measurement of absorbance of TMB in the oxidized form at 450 nm. (B) Plot of inhibition degree of binding between Flt1-F_c and VEGF as a function of EBP block length of anti-Flt1-EBP*n* depending on its concentration in the range of 0.5−500 μM. Each value indicates the mean ± SD obtained from three different experiments independently, $^*P \leq 0.05$, $^{**}P \leq 0.01$, and $^{***}P \leq 0.001$ analyzed by unpaired *t*-test.

between Flt1-F_c and $rhVEGF_{165}$ in a concentration-dependent manner, indicating that anti-Flt1-EBP*n* showed specific binding to Flt1-F_c. In general, as the EBP block length increased in the repeating number range of 3−12, anti-Flt1-EBP*n* largely inhibited binding of Flt1-F_c to $rhVEGF_{165}$, representing that anti-Flt1-EBP*n* maintained specific binding of the anti-Flt1 peptide against Flt1-F_c. It is potentially due to the inert characteristics of EBP pentapeptide repeats, which is in good agreement with the other EBP-based fusion polypeptides.[19,23,24,59] Especially, anti-Flt1-EBP12 at 500 μM showed the maximum inhibition, higher than 75%, while anti-Flt1-EBP24 representing a lower inhibition degree compared with that of anti-Flt1-EBP12 under identical concentration, potentially due to the steric hindrance of the elongated EBP length.[60] The anti-Flt1-EBP*n* in the range of 5−500 μM inhibited the binding of Flt1-Fc to $rhVEGF_{165}$ in a dose-dependent manner, while no significant inhibition was observed at a low concentration below 5.0 μM. Likewise, the chemically synthesized anti-Flt1 peptide as the hexapeptide dose dependently inhibited molecular interactions between $rhVEGF_{165}$ and Flt1-F_c in the range of 10−200 μM.[41] Thus, anti-Flt1-EBP*n* with controlled EBP length showed comparable inhibition of binding of Flt1-F_c to $rhVEGF_{165}$ in the similar concentration range compared with the anti-Flt1 peptide, suggesting that there was minimal interactions between anti-Flt1 peptide and EBP*n*. The biological activities of a variety of functional peptides and proteins conjugated with PEG or genetically fused with EBP to increase the half-life in vivo were maintained as the PEG or EBP block length was optimized, as reported.[31,54]

With anti-Flt1-EBP*n* bound to Flt1 as its antagonist and inhibiting interactions between VEGF and Flt1 as shown in the competitive ELISA, cytotoxicity of anti-Flt1-EBP*n* on HUVECs was evaluated by WST-8 reagent and plotted in Figure 5. When HUVECs were separately treated with EBP12

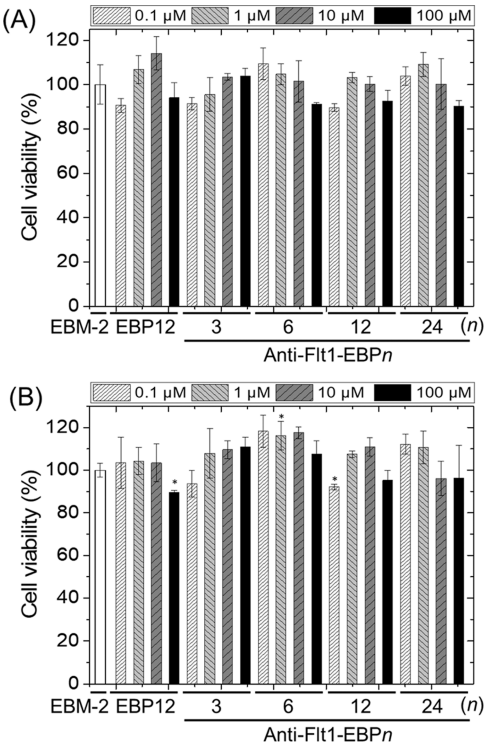

Figure 5. Viability of HUVECs treated with 0.1−100 μM EBP12 as control and anti-Flt1-EBP*n* for (A) 24 and (B) 48 h. The viability of HUVECs was obtained by measuring absorbance at 450 nm from color change of WST-8 reagent. $^*P \leq 0.05$ analyzed by unpaired *t*-test.

as the control and anti-Flt1-EBP*n* in the range of 0.1−100 μM for 24 and 48 h, the medium was replaced with 10% WST-8 solution to quantify cell viability. The viability of HUVECs in EBM-2 as the control was set to be 100%, and the others were normalized. Figure 5A shows that the viability of HUVECs treated with 0.1−100 μM anti-Flt1-EBP*n* was 89.7−109.4%, while that of HUVECs treated with 0.1−100 μM EBP12 was 90.7−114.2% for 24 h. Likewise, as shown in Figure 5B, viability of HUVECs incubated with 0.1−100 μM anti-Flt1-EBP*n* was 92.2−118.3%, while that of HUVECs incubated with 0.1−100 μM EBP12 was 89.6−104.2% for 48 h. It represents that anti-Flt1-EBP*n* as well as EBP12 showed no significant cytotoxicity against HUVECs for 2 days, which is in good agreement with the previous reports that EBPs and their fusion in a soluble state generally have good cell viability.[12,20]

https://doi.org/10.1021/acsami.3c03989
ACS Appl. Mater. Interfaces 2023, 15, 32201−32214

Especially, the EBP length of anti-Flt1-EBP*n* had no large influence on its cytotoxicity in the range of 0.1−100 μM for 48 h. It was reported that the anti-Flt1 peptide inhibited angiogenesis without any suppression of HUVEC proliferation.[41]

Considering that macromolecules exhibited lower clearance in the vitreous[61] and anti-Flt1-EBP*n* showed inhibition in the binding of Flt1-F_c and rhVEGF$_{165}$ in the competitive ELISA without any cytotoxicity against HUVECs, rhVEGF$_{165}$-induced tube formation degree of HUVECs was evaluated with anti-Flt1-EBP*n* at different concentrations to clearly show the effect of EBP length. The HUVECs incubated with rhVEGF$_{165}$ at 50 ng/mL on Matrigel-precoated well-plates were treated with either EBP12 as the control or anti-Flt1-EBP*n* in the range of 0.1−10.0 μM. Figure 6 shows fluorescence images of calcein-AM labeled HUVECs separately incubated with EBP12 or anti-Flt1-EBP*n* in the presence of rhVEGF$_{165}$ and the degree of tube-like network formation depending on the normalized tube length. As represented in Figure 6A, the HUVECs incubated with rhVEGF$_{165}$ showed a higher degree of tube-like network formation than that of HUVECs in the absence of rhVEGF$_{165}$. HUVECs treated with EBP12 in the range of 0.1−10.0 μM as the control showed no significant decrease of tube-like network formation. In contrast, the tube-like network formation of HUVECs treated with anti-Flt1-EBP*n* gradually decreased in a concentration-dependent manner even with rhVEGF$_{165}$. The tube-like network length of HUVECs incubated without or with rhVEGF$_{165}$ was determined to be 0 or 100%, respectively, and that of HUVECs treated with EBP12 or anti-Flt1-EBP*n* was normalized to evaluate the effect of EBP length on tube formation degree of HUVECs, as shown in Figure 5B. The tube formation of HUVECs treated with anti-Flt1-EBP*n* decreased in a concentration-dependent manner, while HUVECs treated with EBP12 in the range of 0.1−10 μM showed a similar degree to that of the rhVEGF$_{165}$-treated HUVECs. The anti-Flt1-EBP3 decreased tube formation of HUVECs in the range of 1−10 μM. Especially, both anti-Flt1-EBP12 and anti-Flt1-EBP24 at 0.1−10 μM showed the most significant decrease of the tube-like network formation of HUVECs. The effective concentration of anti-Flt1-EBP12 in the range of 0.1−10 μM to suppress tube-like network formation of HUVECs was ten times lower than that used in the indirect ELISA to inhibit the binding of Flt1-F_c against rhVEGF$_{165}$ coated at 500 ng/mL on the well. As shown in Figures 4 and 6, anti-Flt1-EBP6 and anti-Flt1-EBP12 at 50−500 μM showed significant inhibition of the binding of Flt1 against rhVEGF$_{165}$, and both anti-Flt1-EBP12 and anti-Flt1-EBP24 at 10 μM showed the most significant suppression of tubing formation of HUVECs. Thus, it suggests that anti-Flt1-EBP12 has an optimized EBP length as the most efficient Flt1 antagonist to inhibit tubing formation of HUVECs, and its inhibitory effect was evaluated compared with that of bevacizumab as a positive control.[39,62]

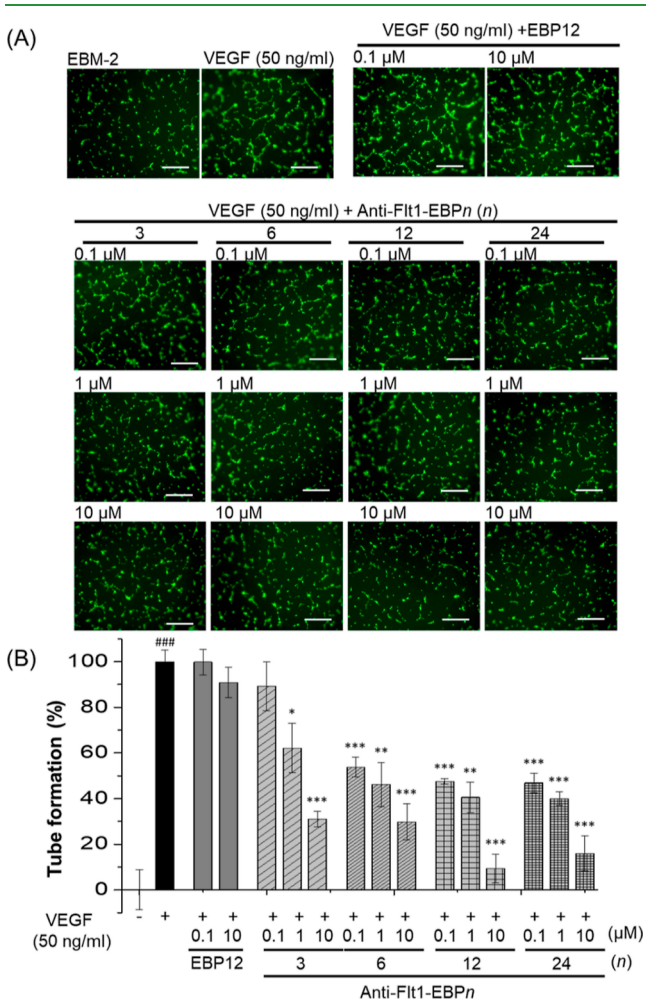

Figure 6. (A) Fluorescence images of HUVECs labeled with calcein-AM and (B) tube formation degree normalized to tube-like network length of HUVECs when they were separately incubated with EBP12 or anti-Flt1-EBP*n* in the presence of rhVEGF$_{165}$. A scale bar in (A) is 500 μm. Tube formation lengths are shown as the mean ± SD obtained from three different experiments independently, $^{*}P \leq 0.05$, $^{**}P \leq 0.01$, and $^{***}P \leq 0.001$ analyzed by unpaired *t*-test.

The anti-angiogenic activity of anti-Flt1-EBP12 on rhVEGF$_{165}$-induced tube formation of HUVECs on Matrigel was assessed compared with FDA-approved bevacizumab. Bevacizumab as a recombinant humanized anti-VEGF monoclonal antibody was studied as control. Bevacizumab specifically bound to rhVEGF$_{165}$, resulting in minimizing rhVEGF$_{165}$-induced tube-like network formation and neovascularization of HUVECs, as reported.[39,62] Figure 7 shows the fluorescence images of HUVECs labeled with calcein-AM and degree of tube-like network formation, depending on normalized tube length obtained from the images, when HUVECs were separately incubated with bevacizumab, EBP12, and anti-Flt1-EBP12 in the presence of rhVEGF$_{165}$. Tube-like network formation of HUVECs incubated with rhVEGF$_{165}$ increased compared with that of HUVECs in the absence of rhVEGF$_{165}$, and tube-like network formation of HUVECs treated with bevacizumab or anti-Flt1-EBP12 largely decreased in a concentration-dependent manner even with rhVEGF$_{165}$, as represented in Figure 7A. In contrast, no substantial inhibition of EBP12 on tube formation of HUVECs was observed under identical conditions. The tube size of HUVECs treated with EBP12 as the control at different concentrations was similar to that of HUVECs under rhVEGF$_{165}$ treatment, as shown in Figure 7B. In contrast, anti-Flt1-EBP12 caused a gradual decrease of the HUVEC tube length in the range of 0.1−10.0 μM, and the tube-like network formation of HUVECs treated with anti-Flt1-EBP12 at 100−200 μM was similar to that of anti-Flt1-EBP12 at 10 μM (data not shown). The degree of tube-like network formation of HUVECs incubated with anti-Flt1-EBP12 at 10.0 μM and rhVEGF$_{165}$ was lower than that of

https://doi.org/10.1021/acsami.3c03989
ACS Appl. Mater. Interfaces 2023, 15, 32201−32214

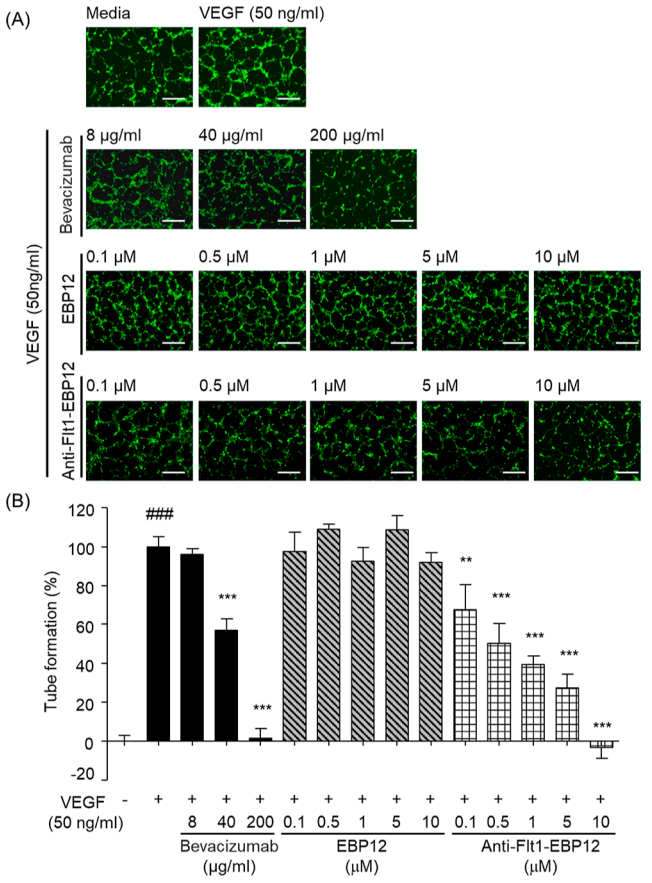

Figure 7. (A) Fluorescence images of HUVECs labeled with calcein-AM and (B) tube formation degree normalized to tube-like network length of HUVECs when they were separately incubated with bevacizumab, EBP12, or anti-Flt1-EBP12 in the presence of $rhVEGF_{165}$. Scale bar in (A) is 500 μm. Tube formation lengths are shown as the mean ± SD obtained from three different experiments independently, $^{*}P \leq 0.05$, $^{**}P \leq 0.01$, and $^{***}P \leq 0.001$ analyzed by unpaired *t*-test.

HUVECs in the absence of $rhVEGF_{165}$. It suggests that the HUVECs treated with anti-Flt1-EBP12 at 10.0 μM even with $rhVEGF_{165}$ migrated and formed tube-like network less than that of HUVECs in the absence of $rhVEGF_{165}$, suggesting that anti-Flt1-EBP12 would be potentially comparable to the anti-Flt1 peptide to inhibit tube formation in vitro, as reported elsewhere.[41] In addition, the degree of tube formation of HUVECs treated with anti-Flt1-EBP12 in the range of 0.1−10.0 μM (3−294 μg/mL) decreased, while HUVECs treated with 8 μg/mL bevacizumab showed no inhibition of tube formation. The lower concentration of anti-Flt1-EBP12 showed enhanced inhibition of tube-like network formation of HUVECs compared to that of bevacizumab, and the degree of tube formation of HUVECs incubated with anti-Flt1-EBP12 at 294 μg/mL exhibited equivalent inhibition degree of the tube formation when bevacizumab at 200 μg/mL was used. As shown by the ELISA results in Figure 4, anti-Flt1-EBP12 maintained specificity of anti-Flt1 peptide against the Flt1 of HUVECs in vitro and showed approximately 100% inhibition of the tube formation at 10 μM, potentially due to the inert characteristics of the EBP block with the optimized chain length.[24,59] Therefore, anti-Flt1-EBP12 would be of great potential to inhibit $rhVEGF_{165}$-triggered angiogenesis.

As shown by its unique LCST behavior, anti-Flt1-EBP12 is completely soluble below its T_t even with poor solubility of the anti-Flt1 peptide in water.[45,46,48] Our results showed that anti-Flt1-EBP12 largely inhibited tube-like network formation of HUVECs without any severe cytotoxicity. Thus, we next investigated the anti-angiogenic effect of anti-Flt1-EBP12 on laser-induced CNV in the wet ARMD mouse model in vivo. Laser irradiation at 532 nm caused the Bruch's membranes to collapse, which induced inflammation to initiate CNV (Figure 8A). A previous study reported that CNV-induced lesions such as retinal pigment epithelium detachment, serious retinal detachment, and formation of fibro-vascular tissue around the CNV area in wet ARMD patients lead to vision loss.[49] In this study, 6−8-week-old female mice were used. Even though retinal neovascular disease usually occurs in elderly people and elderly aged mice (12−16-week-old) exhibit more severe CNV lesion, most studies used adult C57BL/6J female mice (6−8-week-old) because of no difference between sexes and high lesion reproducibility.[63−66] As shown in Figure 8B, IVT of anti-Flt1-EBP12, which is an identical injection method of bevacizumab and aflibercept as an anti-VEGF drug, was immediately performed after laser-mediated injury; the mice were intravitreally injected with PBS or EBP12 as control. The CNV lesions were measured using whole choroidal flat-mounts perfused with FITC-dextran at day 14. Figures 8C,E and 8D,F show fluorescence images of CNV lesions and quantitative analysis of CNV lesion sizes, respectively. The CNV lesion sizes were 0.070 ± 0.021 and 0.050 ± 0.018 mm^2 in mice treated with anti-Flt1-EBP12 (5.0 and 10.0 μg), respectively, and 0.101 ± 0.043 and 0.105 ± 0.037 mm^2 in mice treated with PBS and EBP12 (10 μg), respectively. Anti-Flt1-EBP12 largely reduced the CNV lesion sizes based on those of ARMD mice treated with PBS as the control (30.7% ($P < 0.05$) and 50.5% ($P < 0.001$)). In addition, we investigated the anti-angiogenic effect of aflibercept as a positive control on laser-induced CNV. Aflibercept, which is approved as an anti-VEGF drug, is a decoy receptor fusion protein composed of the third domain of VEGFR2, the second domain of human Flt-1, and the F_c domain of human IgG1.[67] While bevacizumab and ranibizumab have extremely weak interactions with mouse VEGF, aflibercept interacts with mouse VEGF, as reported.[68,69] An experiment, in which aflibercept as a positive control was administered, was conducted under identical conditions to confirm the therapeutic efficacy of anti-Flt1-EBP12. The sizes of CNV lesions by administration of aflibercept (1.0 and 10.0 μg) were 0.041 ± 0.019 and 0.043 ± 0.015 mm^2, respectively, while the CNV size in PBS-treated mice was 0.063 ± 0.019 mm^2. It represents that the CNV lesion sizes were reduced by 35.0 and 31.7% compared to the PBS control group, as shown in Figure 8E,F. Thus, anti-Flt1-EBP12 showed similar therapeutic efficacy depending on the dose even on indirect comparison with aflibercept.

Previously, systemic distribution of intravitreally injected anti-VEGF agents, bevacizumab and aflibercept, was figured out by using I124-labeled agents and positron emission tomography−computed tomography imaging. Although bevacizumab and aflibercept were in the vitreous for more than 20 days, they were directly diffused to serum within 1 h and localized in the liver, heart, and distal femur bones.[70] In addition, to investigate the distribution of EBP, rhodamine-labeled EBP was intravenously administered, representing that the EBPs were mainly accumulated in kidneys, followed by the liver by ex vivo imaging of the whole organ.[28] Especially, to

https://doi.org/10.1021/acsami.3c03989
ACS Appl. Mater. Interfaces 2023, 15, 32201−32214

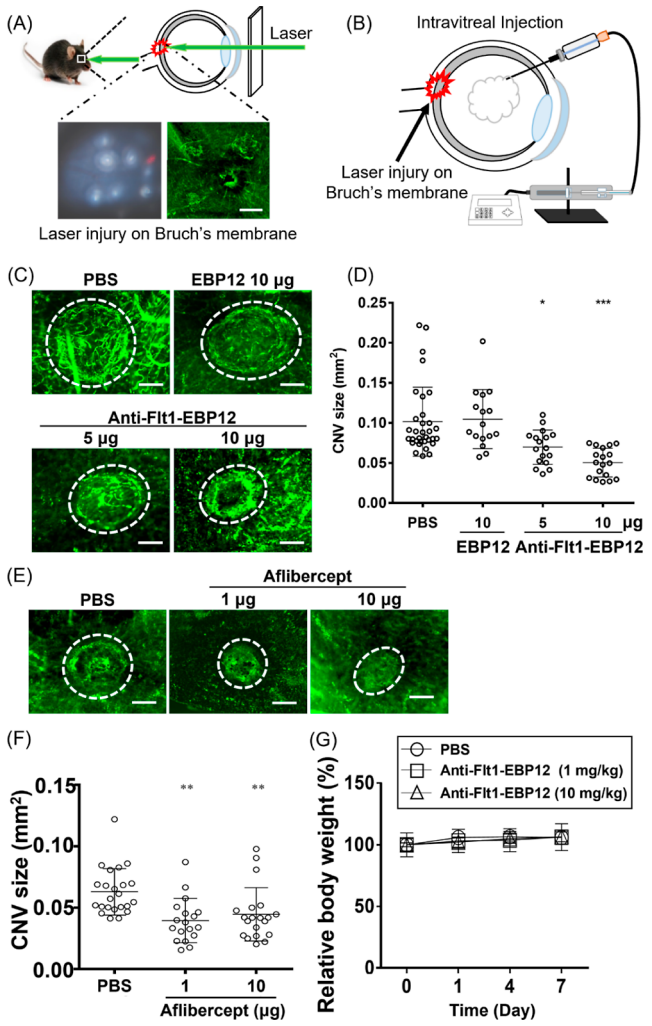

Figure 8. (A) Schematic of the application of laser irradiation at 532 nm to cause Bruch's membrane to collapse. Multiple burns were executed by a diode laser emitting a wavelength of 532 nm (210 mW, 0.1 s, and 100 μm) to each fundus in vivo. A scale bar indicates 50 μm. (B) Schematic of IVT of anti-Flt1-EBP12 after laser injury to investigate suppression of laser-triggered CNV in the wet ARMD mice model. The mice were intravitreally injected with PBS, EBP12 (10 μg), and anti-Flt1-EBP12 (5 and 10 μg) (n = 4 per group) once immediately after laser injury. (C,E) Fluorescence microscopic images of the choroidal flat mounts of the CNV lesions marked with white dotted circles and (D,F) plots of the CNV lesion size of each group as a function of the injected amount of anti-Flt1-EBP12 and aflibercept in total when the whole choroidal flat mounts of the euthanized mice were perfused with FITC-conjugated dextran (MW 2000 kDa) on day 14. The lesion size was measured using a nanozoomer and FISH. Each point indicates its size while the horizontal bar represents the mean ± SD of a group, $^{*}P \leq 0.05$, $^{**}P < 0.01$, and $^{***}P < 0.001$ by one-way ANOVA plus Tukey's test. (G) Relative body weight (%) of each group as a function of time for systemic toxicity of anti-Flt1-EBP12. The mice (n = 3 per group) were intra-peritoneally injected with PBS as control and anti-Flt1-EBP12 (1 and 10 mg/kg) and observed for 1 week.

evaluate systemic toxicity of anti-Flt1-EBP12, the acute toxicity test was performed to investigate its biosafety. As reported,[71−73] the drug is intra-peritoneally administered once, and mortality, body weight, and behavioral changes of the mice are observed for 7 days to test any acute toxicity. A single intraperitoneal injection of anti-Flt1-EBP12 had no effect on mice survival. No changes such as hair loss, decreased activity, and decreased excretion were observed on checking the appearance of the mice. Figure 8G shows that the body weight of mice slightly increased in all groups compared to that before administration, and there was no large difference between the anti-Flt1-EBP12-treated group and the PBS one as control. It suggests that anti-Flt1-EBP12 had no significant acute toxicity in vivo for 7 days and could be a potential therapeutic candidate for the treatment of wet ARMD even though pharmacokinetic and pharmacodynamic investigation is needed to validate the effect of anti-Flt1-EBP12 on wet ARMD. In addition, the half-life of anti-Flt1-EBP12 and anti-Flt1 peptide as the control will be studied by using the ELISA method, in which they are conjugated with biotin and detected with streptavidin-horse radish peroxidase antibody. The amount of biotin-conjugated anti-Flt1-EBP12 remaining in the eye after intraocular injection will be measured to determine the degree of intraocular retention.[74]

CONCLUSIONS

A series of anti-Flt1-EBPn fusion polypeptides with the anti-Flt1 peptide for Flt1 targeting and a thermally responsive EBP block having four different block lengths were genetically engineered, bio-synthesized in a bacterial expression system, and non-chromatographically separated with high purity. We explored the potential therapeutic applications of these fusion polypeptides to treat angiogenesis diseases including diabetic retinopathy and cancer. As shown by the ELISA results, the anti-Flt1-EBPn in a soluble unimer form under physiological conditions significantly inhibited binding between VEGF and Flt1 in a concentration-dependent manner, potentially due to its high binding affinity with Flt1. Especially, anti-Flt1-EBP12 with the optimized EBP length showed the maximum inhibition because the optimized EBP block length allowed the anti-Flt1 peptide at the N terminal to have spatial specific binding to Flt1. Anti-Flt1-EBP12 significantly inhibited tube-like network formation of HUVECs in vitro on the condition of Flt1-mediated angiogenesis via VEGF binding and its inhibition degree was comparable to that of the humanized anti-VEGF mAb. Finally, anti-Flt1-EBP12 showed high anti-neovascularization effect on CNV in the wet ARMD mice as models of retinal neovascularization-related diseases. Therefore, these EBP fusion polypeptides with the anti-Flt1 peptide have great potential as the receptor-targeted therapeutic polypeptides for anti-angiogenesis purposes to treat neovascularization-related diseases in retina, cornea, and choroid. These fusion polypeptides show advantages as they are rationally designed genetically, bio-synthesized by bacterial expression systems, easily purified non-chromatographically by thermal-triggering of EBP blocks for large-scale production, and have biocompatibility as well as low immunogenicity, as reported.[14] Potentially, it represents that any receptor targeting peptides screened by either phage display library or synthetic peptide combinatorial one would be genetically fused with a biologically inert EBP block with an optimal chain length like PEG−peptide conjugates so that the receptor targeting peptide−EBP fusion polypeptides as the receptor antagonists would be effective to control over a number of receptor-mediated biological processes.[24]

https://doi.org/10.1021/acsami.3c03989
ACS Appl. Mater. Interfaces 2023, 15, 32201−32214

AUTHOR INFORMATION

Corresponding Authors

SaeGwang Park − *Department of Microbiology and Immunology, College of Medicine, Inje University, Busan 47392, Republic of Korea*; Email: micpsg@inje.ac.kr

Dong Woo Lim − *Department of Bionano Engineering and Department of Bionanotechnology, Center for Bionano Intelligence Education and Research, Hanyang University, Ansan 15588, Republic of Korea*; orcid.org/0000-0003-2887-268X; Email: dlim@hanyang.ac.kr

Authors

Min Jeong Kang − *Department of Bionano Engineering and Department of Bionanotechnology, Center for Bionano Intelligence Education and Research, Hanyang University, Ansan 15588, Republic of Korea*

Kug-Hwan Roh − *Department of Microbiology and Immunology, College of Medicine, Inje University, Busan 47392, Republic of Korea*

Jae Sang Lee − *Department of Bionano Engineering and Department of Bionanotechnology, Center for Bionano Intelligence Education and Research, Hanyang University, Ansan 15588, Republic of Korea*

Jae Hee Lee − *Department of Bionano Engineering and Department of Bionanotechnology, Center for Bionano Intelligence Education and Research, Hanyang University, Ansan 15588, Republic of Korea*

Complete contact information is available at: https://pubs.acs.org/10.1021/acsami.3c03989

Notes

The authors declare no competing financial interest.

ACKNOWLEDGMENTS

This work was supported by the National Research Foundation (NRF) of Korea funded by the Ministry of Science and ICT, Korea (2021R1A2C1010682) and the Ministry of Education, Korea (2018R1A6A1A03024231).

REFERENCES

(1) Kinch, M. S. An Overview of FDA-Approved Biologics Medicines. *Drug discovery today* **2015**, *20*, 393−398.

(2) Bobo, D.; Robinson, K. J.; Islam, J.; Thurecht, K. J.; Corrie, S. R. Nanoparticle-Based Medicines: A Review of Fda-Approved Materials and Clinical Trials to Date. *Pharm. Res.* **2016**, *33*, 2373−2387.

(3) Vivès, E.; Schmidt, J.; Pèlegrin, A. Cell-Penetrating and Cell-Targeting Peptides in Drug Delivery. *Biochim. Biophys. Acta, Rev. Cancer* **2008**, *1786*, 126−138.

(4) Gaspar, D.; Veiga, A. S.; Castanho, M. A. From Antimicrobial to Anticancer Peptides. A Review. *Front. Microbiol.* **2013**, *4*, 294.

(5) Epand, R. M. Fusion Peptides and the Mechanism of Viral Fusion. *Biochim. Biophys. Acta, Biomembr.* **2003**, *1614*, 116−121.

(6) Yu, K.; Liu, C.; Kim, B. G.; Lee, D. Y. Synthetic Fusion Protein Design and Applications. *Biotechnol. Adv.* **2015**, *33*, 155−164.

(7) Meyer, D. E.; Chilkoti, A. Genetically Encoded Synthesis of Protein-Based Polymers with Precisely Specified Molecular Weight and Sequence by Recursive Directional Ligation: Examples from the Elastin-Like Polypeptide System. *Biomacromolecules* **2002**, *3*, 357−367.

(8) Young, C. L.; Britton, Z. T.; Robinson, A. S. Recombinant Protein Expression and Purification: A Comprehensive Review of Affinity Tags and Microbial Applications. *Biotechnol. J.* **2012**, *7*, 620−634.

(9) Padlan, E. A. A Possible Procedure for Reducing the Immunogenicity of Antibody Variable Domains While Preserving Their Ligand-Binding Properties. *Mol. Immunol.* **1991**, *28*, 489−498.

(10) Lee, J.; Kim, J.; Hwang, S.; Lee, W.; Yoon, H.; Lee, H.; Hong, S. High-Level Expression of Antimicrobial Peptide Mediated by a Fusion Partner Reinforcing Formation of Inclusion Bodies. *Biochem. Biophys. Res. Commun.* **2000**, *277*, 575−580.

(11) Shah, A.; Malik, M. S.; Khan, G. S.; Nosheen, E.; Iftikhar, F. J.; Khan, F. A.; Shukla, S. S.; Akhter, M. S.; Kraatz, H.-B.; Aminabhavi, T. M. Stimuli-Responsive Peptide-Based Biomaterials as Drug Delivery Systems. *Chem. Eng. J.* **2018**, *353*, 559−583.

(12) MacEwan, S. R.; Chilkoti, A. Applications of Elastin-Like Polypeptides in Drug Delivery. *J. Controlled Release* **2014**, *190*, 314−330.

(13) MacEwan, S. R.; Chilkoti, A. Elastin-Like Polypeptides: Biomedical Applications of Tunable Biopolymers. *Pept. Sci.* **2010**, *94*, 60−77.

(14) Kim, W.; Chaikof, E. L. Recombinant Elastin-Mimetic Biomaterials: Emerging Applications in Medicine. *Adv. Drug Delivery Rev.* **2010**, *62*, 1468−1478.

(15) Wright, E. R.; McMillan, R. A.; Cooper, A.; Apkarian, R. P.; Conticello, V. P. Thermoplastic Elastomer Hydrogels Via Self-Assembly of an Elastin-Mimetic Triblock Polypeptide. *Adv. Funct. Mater.* **2002**, *12*, 149−154.

(16) Li, N. K.; Quiroz, F. G.; Hall, C. K.; Chilkoti, A.; Yingling, Y. G. Molecular Description of the LCST Behavior of an Elastin-Like Polypeptide. *Biomacromolecules* **2014**, *15*, 3522−3530.

(17) Meyer, D. E.; Trabbic-Carlson, K.; Chilkoti, A. Protein Purification by Fusion with an Environmentally Responsive Elastin-Like Polypeptide: Effect of Polypeptide Length on the Purification of Thioredoxin. *Biotechnol. Prog.* **2001**, *17*, 720−728.

(18) Hassouneh, W.; Christensen, T.; Chilkoti, A. Elastin-Like Polypeptides as a Purification Tag for Recombinant Proteins. *Curr. Protoc. Protein Sci.* **2010**, *61*, 6.11. 1−6.11. 16.

(19) Gao, W.; Liu, W.; Christensen, T.; Zalutsky, M. R.; Chilkoti, A. In Situ Growth of a PEG-Like Polymer from the C Terminus of an Intein Fusion Protein Improves Pharmacokinetics and Tumor Accumulation. *Proc. Natl. Acad. Sci. U.S.A.* **2010**, *107*, 16432−16437.

(20) McDaniel, J. R.; Bhattacharyya, J.; Vargo, K. B.; Hassouneh, W.; Hammer, D. A.; Chilkoti, A. Self-Assembly of Thermally Responsive Nanoparticles of a Genetically Encoded Peptide Polymer by Drug Conjugation. *Angew. Chem., Int. Ed. Engl.* **2013**, *52*, 1683−1687.

(21) Asai, D.; Xu, D.; Liu, W.; Garcia Quiroz, F.; Callahan, D. J.; Zalutsky, M. R.; Craig, S. L.; Chilkoti, A. Protein Polymer Hydrogels by in Situ, Rapid and Reversible Self-Gelation. *Biomaterials* **2012**, *33*, 5451−5458.

(22) Hu, J.; Wang, G.; Liu, X.; Gao, W. Enhancing Pharmacokinetics, Tumor Accumulation, and Antitumor Efficacy by Elastin-Like Polypeptide Fusion of Interferon Alpha. *Adv. Mater.* **2015**, *27*, 7320−7324.

(23) Gilroy, C. A.; Roberts, S.; Chilkoti, A. Fusion of Fibroblast Growth Factor 21 to a Thermally Responsive Biopolymer Forms an Injectable Depot with Sustained Anti-Diabetic Action. *J. Controlled Release* **2018**, *277*, 154−164.

(24) Shamji, M. F.; Jing, L.; Chen, J.; Hwang, P.; Ghodsizadeh, O.; Friedman, A. H.; Richardson, W. J.; Setton, L. A. Treatment of Neuroinflammation by Soluble Tumor Necrosis Factor Receptor Type Ii Fused to a Thermally Responsive Carrier. *J. Neurosurg.* **2008**, *9*, 221−228.

(25) Sreekumar, P. G.; Li, Z.; Wang, W.; Spee, C.; Hinton, D. R.; Kannan, R.; MacKay, J. A. Intra-vitreal αB crystallin fused to elastin-like polypeptide provides neuroprotection in a mouse model of age-related macular degeneration. *J. Controlled Release* **2018**, *283*, 94−104.

(26) Wang, W.; Jashnani, A.; Aluri, S. R.; Gustafson, J. A.; Hsueh, P.-Y.; Yarber, F.; McKown, R. L.; Laurie, G. W.; Hamm-Alvarez, S. F.; MacKay, J. A. A Thermo-Responsive Protein Treatment for Dry Eyes. *J. Controlled Release* **2015**, *199*, 156−167.

(27) Wada, I.; Sreekumar, P. G.; Spee, C.; MacKay, A. J.; Ip, M.; Kannan, R. Mechanisms of Epithelial-Mesenchymal Transition and

Prevention of Dispase-Induced PVR by Delivery of an Antioxidant αB Crystallin Peptide. *Antioxidants* **2022**, *11*, 2080.
(28) Kuna, M.; Mahdi, F.; Chade, A. R.; Bidwell, G. L. Molecular Size Modulates Pharmacokinetics, Biodistribution, and Renal Deposition of the Drug Delivery Biopolymer Elastin-Like Polypeptide. *Sci. Rep.* **2018**, *8*, 7923−8012.
(29) Meyer, D. E.; Chilkoti, A. Quantification of the Effects of Chain Length and Concentration on the Thermal Behavior of Elastin-Like Polypeptides. *Biomacromolecules* **2004**, *5*, 846−851.
(30) McDaniel, J. R.; MacEwan, S. R.; Li, X.; Radford, D. C.; Landon, C. D.; Dewhirst, M.; Chilkoti, A. Rational Design of "Heat Seeking" Drug Loaded Polypeptide Nanoparticles That Thermally Target Solid Tumors. *Nano Lett.* **2014**, *14*, 2890−2895.
(31) Shamji, M. F.; Betre, H.; Kraus, V. B.; Chen, J.; Chilkoti, A.; Pichika, R.; Masuda, K.; Setton, L. A. Development and Characterization of a Fusion Protein between Thermally Responsive Elastin-Like Polypeptide and Interleukin-1 Receptor Antagonist: Sustained Release of a Local Antiinflammatory Therapeutic. *Arthritis Rheum.* **2007**, *56*, 3650−3661.
(32) Carmeliet, P.; Jain, R. K. Angiogenesis in Cancer and Other Diseases. *nature* **2000**, *407*, 249−257.
(33) Aiello, L. P.; Pierce, E. A.; Foley, E. D.; Takagi, H.; Chen, H.; Riddle, L.; Ferrara, N.; King, G. L.; Smith, L. Suppression of Retinal Neovascularization in Vivo by Inhibition of Vascular Endothelial Growth Factor (VEGF) Using Soluble Vegf-Receptor Chimeric Proteins. *Proc. Natl. Acad. Sci. U.S.A.* **1995**, *92*, 10457−10461.
(34) Bai, Y.-J.; Huang, L.-Z.; Xu, X.-L.; Du, W.; Zhou, A.-Y.; Yu, W.-Z.; Li, X.-X. Polyethylene Glycol-Modified Pigment Epithelial-Derived Factor: New Prospects for Treatment of Retinal Neovascularization. *J. Pharmacol. Exp. Ther.* **2012**, *342*, 131−139.
(35) Gao, G.; Shao, C.; Zhang, S.; Dudley, A.; Fant, J.; Ma, J.-X. Kallikrein-Binding Protein Inhibits Retinal Neovascularization and Decreases Vascular Leakage. *Diabetologia* **2003**, *46*, 689−698.
(36) V Rosca, E.; E Koskimaki, J.; G Rivera, C.; B Pandey, N.; P Tamiz, A.; S Popel, A. Anti-Angiogenic Peptides for Cancer Therapeutics. *Curr. Pharm. Biotechnol.* **2011**, *12*, 1101−1116.
(37) Zhang, D.; Kaufman, P.; Gao, G.; Saunders, R.; Ma, J. Intravitreal Injection of Plasminogen Kringle 5, an Endogenous Angiogenic Inhibitor, Arrests Retinal Neovascularization in Rats. *Diabetologia* **2001**, *44*, 757−765.
(38) Longeras, R.; Farjo, K.; Ihnat, M.; Ma, J.-X. A PEDF-Derived Peptide Inhibits Retinal Neovascularization and Blocks Mobilization of Bone Marrow-Derived Endothelial Progenitor Cells. *Exp. Diabetes Res.* **2012**, *2012*, 518426.
(39) Avery, R. L.; Pieramici, D. J.; Rabena, M. D.; Castellarin, A. A.; Nasir, M. A.; Giust, M. J. Intravitreal Bevacizumab (Avastin) for Neovascular Age-Related Macular Degeneration. *Ophthalmology* **2006**, *113*, 363−372.
(40) Suzuma, K.; Naruse, K.; Suzuma, I.; Takahara, N.; Ueki, K.; Aiello, L. P.; King, G. L. Vascular Endothelial Growth Factor Induces Expression of Connective Tissue Growth Factor Via KDR, Flt1, and Phosphatidylinositol 3-Kinase-Akt-Dependent Pathways in Retinal Vascular Cells. *J. Biol. Chem.* **2000**, *275*, 40725−40731.
(41) Bae, D.-G.; Kim, T.-D.; Li, G.; Yoon, W.-H.; Chae, C.-B. Anti-Flt1 Peptide, a Vascular Endothelial Growth Factor Receptor 1−Specific Hexapeptide, Inhibits Tumor Growth and Metastasis. *Clin. Cancer Res.* **2005**, *11*, 2651−2661.
(42) Kim, H.; Choi, J.-S.; Kim, K. S.; Yang, J.-A.; Joo, C.-K.; Hahn, S. K. Flt1 Peptide−Hyaluronate Conjugate Micelle-Like Nanoparticles Encapsulating Genistein for the Treatment of Ocular Neovascularization. *Acta Biomater.* **2012**, *8*, 3932−3940.
(43) Kim, M. H.; Kim, S.-G.; Kim, D.-W. Tc-99m and Fluorescence-Labeled Anti-Flt1 Peptide as a Multimodal Tumor Imaging Agent Targeting Vascular Endothelial Growth Factor-Receptor 1. *Nucl. Med. Mol. Imaging* **2018**, *52*, 359−367.
(44) Kong, J.-S.; Yoo, S.-A.; Kang, J.-H.; Ko, W.; Jeon, S.; Chae, C.-B.; Cho, C.-S.; Kim, W.-U. Suppression of Neovascularization and Experimental Arthritis by D-Form of Anti-Flt-1 Peptide Conjugated with Mini-PEG. *Angiogenesis* **2011**, *14*, 431−442.
(45) Li, Q.; Zhou, R.; Sun, Y.; Xiao, D.; Liu, M.; Zhao, D.; Peng, S.; Chen, Y.; Lin, Y. Synthesis and Antitumor Application of Antiangiogenetic Gold Nanoclusters. *ACS Appl. Mater. Interfaces* **2021**, *13*, 11708−11720.
(46) Oh, E. J.; Choi, J.-S.; Kim, H.; Joo, C.-K.; Hahn, S. K. Anti-Flt1 Peptide−Hyaluronate Conjugate for the Treatment of Retinal Neovascularization and Diabetic Retinopathy. *Biomaterials* **2011**, *32*, 3115−3123.
(47) Oh, E. J.; Park, K.; Choi, J.-S.; Joo, C.-K.; Hahn, S. K. Synthesis, Characterization, and Preliminary Assessment of Anti-Flt1 Peptide−Hyaluronate Conjugate for the Treatment of Corneal Neovascularization. *Biomaterials* **2009**, *30*, 6026−6034.
(48) Seo, S. J.; Lee, S. H.; Kim, K. H.; Kim, J. K. Anti-Flt1 Peptide and Cyanine-Conjugated Gold Nanoparticles for the Concurrent Antiangiogenic and Endothelial Cell Proton Treatment. *J. Biomed. Mater. Res., Part B* **2019**, *107*, 1272−1283.
(49) Shah, R. S.; Soetikno, B. T.; Lajko, M.; Fawzi, A. A. A Mouse Model for Laser-Induced Choroidal Neovascularization. *J. Visualized Exp.* **2015**, *106*, No. e53502.
(50) Basheer, A.; Shahid, S.; Kang, M. J.; Lee, J. H.; Lee, J. S.; Lim, D. W. Switchable Self-Assembly of Elastin-and Resilin-Based Block Copolypeptides with Converse Phase Transition Behaviors. *ACS Appl. Mater. Interfaces* **2021**, *13*, 24385−24400.
(51) Lee, J. S.; Kang, M. J.; Lee, J. H.; Lim, D. W. Injectable Hydrogels of Stimuli-Responsive Elastin and Calmodulin-Based Triblock Copolypeptides for Controlled Drug Release. *Biomacromolecules* **2022**, *23*, 2051−2063.
(52) Kim, H. W.; Roh, K.-H.; Kim, S. W.; Park, S. J.; Lim, N.-Y.; Jung, H.; Choi, I.-W.; Park, S. Type I pig collagen enhances the efficacy of PEDF 34-mer peptide in a mouse model of laser-induced choroidal neovascularization. *Graefe's Arch. Clin. Exp. Ophthalmol.* **2019**, *257*, 1709−1717.
(53) Urry, D. W. Physical Chemistry of Biological Free Energy Transduction as Demonstrated by Elastic Protein-Based Polymers. *J. Phys. Chem. B* **1997**, *101*, 11007−11028.
(54) Chiu, K.; Agoubi, L. L.; Lee, I.; Limpar, M. T.; Lowe, J. W., Jr; Goh, S. L. Effects of Polymer Molecular Weight on the Size, Activity, and Stability of PEG-Functionalized Trypsin. *Biomacromolecules* **2010**, *11*, 3688−3692.
(55) Christensen, T.; Amiram, M.; Dagher, S.; Trabbic-Carlson, K.; Shamji, M. F.; Setton, L. A.; Chilkoti, A. Fusion Order Controls Expression Level and Activity of Elastin-Like Polypeptide Fusion Proteins. *Protein Sci.* **2009**, *18*, 1377−1387.
(56) Lim, D. W.; Trabbic-Carlson, K.; MacKay, J. A.; Chilkoti, A. Improved Non-Chromatographic Purification of a Recombinant Protein by Cationic Elastin-Like Polypeptides. *Biomacromolecules* **2007**, *8*, 1417−1424.
(57) Chaudhuri, R.; Cheng, Y.; Middaugh, C. R.; Volkin, D. B. High-Throughput Biophysical Analysis of Protein Therapeutics to Examine Interrelationships between Aggregate Formation and Conformational Stability. *AAPS J.* **2014**, *16*, 48−64.
(58) Meyer, D. E.; Chilkoti, A. Purification of Recombinant Proteins by Fusion with Thermally-Responsive Polypeptides. *Nat. Biotechnol.* **1999**, *17*, 1112−1115.
(59) Pesce, D.; Wu, Y.; Kolbe, A.; Weil, T.; Herrmann, A. Enhancing Cellular Uptake of GFP Via Unfolded Supercharged Protein Tags. *Biomaterials* **2013**, *34*, 4360−4367.
(60) Khandare, J.; Minko, T. Polymer−Drug Conjugates: Progress in Polymeric Prodrugs. *Prog. Polym. Sci.* **2006**, *31*, 359−397.
(61) Del Amo, E. M.; Rimpelä, A.-K.; Heikkinen, E.; Kari, O. K.; Ramsay, E.; Lajunen, T.; Schmitt, M.; Pelkonen, L.; Bhattacharya, M.; Richardson, D.; et al. Pharmacokinetic Aspects of Retinal Drug Delivery. *Prog. Retinal Eye Res.* **2017**, *57*, 134−185.
(62) Ferrara, N.; Hillan, K. J.; Novotny, W. Bevacizumab (Avastin), a Humanized Anti-VEGF Monoclonal Antibody for Cancer Therapy. *Biochem. Biophys. Res. Commun.* **2005**, *333*, 328−335.
(63) Espinosa-Heidmann, D. G.; Marin-Castano, M. E.; Pereira-Simon, S.; Hernandez, E. P.; Elliot, S.; Cousins, S. W. Gender and

Estrogen Supplementation Increases Severity of Experimental Choroidal Neovascularization. *Exp. Eye Res.* **2005**, *80*, 413−423.
(64) Espinosa-Heidmann, D. G.; Suner, I.; Hernandez, E. P.; Frazier, W. D.; Csaky, K. G.; Cousins, S. W. Age as an Independent Risk Factor for Severity of Experimental Choroidal Neovascularization. *Invest. Ophthalmol. Visual Sci.* **2002**, *43*, 1567−1573.
(65) Gong, Y.; Li, J.; Sun, Y.; Fu, Z.; Liu, C.-H.; Evans, L.; Tian, K.; Saba, N.; Fredrick, T.; Morss, P.; et al. Optimization of an Image-Guided Laser-Induced Choroidal Neovascularization Model in Mice. *PLoS One* **2015**, *10*, No. e0132643.
(66) Lambert, V.; Lecomte, J.; Hansen, S.; Blacher, S.; Gonzalez, M.-L. A.; Struman, I.; Sounni, N. E.; Rozet, E.; De Tullio, P.; Foidart, J. M.; et al. Laser-Induced Choroidal Neovascularization Model to Study Age-Related Macular Degeneration in Mice. *Nat. Protoc.* **2013**, *8*, 2197−2211.
(67) Semeraro, F.; Morescalchi, F.; Duse, S.; Parmeggiani, F.; Gambicorti, E.; Costagliola, C. Aflibercept in Wet Amd: Specific Role and Optimal Use. *Drug Des., Dev. Ther.* **2013**, 711−722.
(68) Ichiyama, Y.; Matsumoto, R.; Obata, S.; Sawada, O.; Saishin, Y.; Kakinoki, M.; Sawada, T.; Ohji, M. Assessment of Mouse VEGF Neutralization by Ranibizumab and Aflibercept. *PLoS One* **2022**, *17*, No. e0278951.
(69) Yu, L.; Wu, X.; Cheng, Z.; Lee, C. V.; LeCouter, J.; Campa, C.; Fuh, G.; Lowman, H.; Ferrara, N. Interaction between Bevacizumab and Murine Vegf-A: A Reassessment. *Invest. Ophthalmol. Visual Sci.* **2008**, *49*, 522−527.
(70) Christoforidis, J. B.; Briley, K.; Binzel, K.; Bhatia, P.; Wei, L.; Kumar, K.; Knopp, M. V. Systemic Biodistribution and Intravitreal Pharmacokinetic Properties of Bevacizumab, Ranibizumab, and Aflibercept in a Nonhuman Primate Model. *Invest. Ophthalmol. Visual Sci.* **2017**, *58*, 5636−5645.
(71) Li, J.-j.; Cona, M. M.; Feng, Y.-b.; Chen, F.; Zhang, G.-z.; Fu, X.-b.; Himmelreich, U.; Oyen, R.; Verbruggen, A.; Ni, Y.-c. A Single-Dose Toxicity Study on Non-Radioactive Iodinated Hypericin for a Targeted Anticancer Therapy in Mice. *Acta Pharmacol. Sin.* **2012**, *33*, 1549−1556.
(72) Ponnapakkam, T.; Bongay-Williams, K.; Beamon, T.; Hooks, R.; Cheatham, D.; Goyal, N.; Anbalagan, M.; Foroozesh, M. Acute Toxicity Evaluation of a Novel Ceramide Analog for the Treatment of Breast Cancer. *Toxicol. Rep.* **2021**, *8*, 1521−1526.
(73) Shiga, A.; Kakamu, S.; Sugiyama, Y.; Shibata, M.; Makino, E.; Enomoto, M. Acute Toxicity of Pierisin-1, a Cytotoxic Protein from Pieris Rapae, in Mouse and Rat. *J. Toxicol. Sci.* **2006**, *31*, 123−137.
(74) Luong, J. H.; Vashist, S. K. Chemistry of Biotin−Streptavidin and the Growing Concern of an Emerging Biotin Interference in Clinical Immunoassays. *ACS Omega* **2019**, *5*, 10−18.

https://doi.org/10.1021/acsami.3c03989
ACS Appl. Mater. Interfaces 2023, 15, 32201−32214